

## A Monte Carlo Study of Peptide Insertion into Lipid Bilayers: Equilibrium Conformations and Insertion Mechanisms

Michael W. Maddox and Marjorie L. Longo

Department of Chemical Engineering and Materials Science, University of California, Davis, California 95616 USA

**ABSTRACT** The membrane insertion behavior of two peptides, Magainin2 and M2 $\delta$ , was investigated by applying the Monte Carlo simulation technique to a theoretical model. The model included many novel aspects, such as a new semi-empirical lipid bilayer model and a new set of semi-empirical transfer energies, which reproduced the experimental insertion behavior of Magainin2 and M2 $\delta$  without parameter fitting. Additionally, we have taken into account diminished internal (intramolecular) hydrogen bonding at the N- and C-termini of helical peptides. All simulations were carried out at 305 K, above the membrane thermal phase transition temperature, and at pH 7.0. The peptide equilibrium conformations are discussed for a range of bilayers with tail polarities varying from octanol-like to alkane-like. Probability distributions of the individual amino-acid-residue positions show the dynamic nature of these equilibrium conformations. Two different insertion mechanisms for M2 $\delta$ , and a translocation mechanism for Magainin2, are described. A study of the effect of bilayer thickness on M2 $\delta$  insertion suggests a critical thickness above which insertion is unfavorable. Additionally, we did not need to use an orientational potential or array of hard cylinders to persuade M2 $\delta$  to insert perpendicular to the membrane surface. Instead, we found that diminished internal hydrogen bonding in the helical conformation anchored the termini in the headgroups and resulted in a nearly perpendicular orientation.

### INTRODUCTION

Membrane peptides (and proteins) mediate many important cell processes, including signal transduction, viral infection, cell aggregation, membrane fusion, and membrane rupture (lysing). The peptide's function is dependent on its position and conformation within the membrane, which is controlled by a large number of system variables. Typical conformations include one or more  $\alpha$ -helical segments that can span the lipid bilayer or adsorb to the bilayer surface. Although many different membrane/peptide systems have been investigated, both experimentally and theoretically, our understanding of the microscopic relationships underlying the observed behaviors is still far from complete. A better understanding of the way in which system parameters affect peptide adsorption, insertion, conformation, and membrane fusion and lysis, would be invaluable in the optimization of these behaviors for biotechnological and pharmaceutical applications.

Experimental studies provide most of our information about membrane/peptide systems, including peptide orientation and depth of penetration (i.e., does the peptide insert), and changes to the bilayer, such as surface area expansion, membrane leakage, rupture and fusion (for a few examples, see Griffith et al., 1974; McIntosh and Simon, 1993; Ho et al., 1995; Longo et al., 1997, 1998; Channareddy and Janes, 1999; Zhou et al., 2000; Nicol et al., 2000). Although some molecular-level interactions can be inferred from experi-

ment, theoretical work is required in conjunction with these results to develop and test detailed molecular-level theories.

The behavior of a membrane/peptide system is controlled by the properties of the peptide/solvent phase, properties of the membrane, and global properties such as temperature and pH. Several theoretical studies have concentrated on the effects of membrane properties on peptide insertion behavior, representing the peptides as simplified solid inclusions of varying geometries. Although they require a number of approximations and generalizations to be tractable, and give no mechanistic information, these models show that lipid composition (which encompasses membrane thickness, density, spontaneous curvature, and bending stiffness), inclusion/membrane thickness mismatches, and the presence of membrane soluble solutes, as well as peptide properties such as concentration in solution, inclusion conformation (geometry), and inclusion hydrophobicity, can all affect the thermodynamic equilibrium state of a membrane/peptide system (Dan and Safran, 1995, 1998; Dan, 1996; Cantor, 1999; Chou et al., 2001). In contrast, peptide folding and the nature of the hydrophobic and polar interactions of peptides with the head and tail regions of the bilayer are emphasized in other theoretical studies of membrane/peptide systems. These include purely theoretical studies (Engelman et al., 1986), statistical mechanical studies (Milik and Skolnick, 1992; Ben-Shaul et al., 1996), Monte Carlo (MC) simulation studies (Milik and Skolnick, 1993, 1995; Baumgaertner, 1996; Sintes and Baumgaertner, 1998; Efremov et al., 1999a,b), and molecular dynamics (MD) simulation studies (Berneche et al., 1998; Lin and Baumgaertner, 2000). These researchers propose several different models, each of which predicts peptide chain behavior (insertion, adsorption, orientation, etc.) in agreement with experimental results for the same systems. These studies show the relationship between

*Received for publication 3 April 2001 and in final form 10 October 2001.*

Address reprint requests to Marjorie L. Longo, Dept. of Chemical Engineering and Materials Science, University of California, Davis, CA 95616. Tel.: 530-754-6348; Fax: 530-752-1031; E-mail: mllongo@ucdavis.edu.

© 2002 by the Biophysical Society

0006-3495/02/01/244/20 \$2.00

peptide amino-acid composition and the preferred equilibrium state, as well as providing information about mechanistic pathways.

Computer simulations of biological systems can be divided into two general classes; a full-atom model, containing as much detail as possible, and a coarse-grained approximation, containing only those details relevant to the properties of interest. MD simulations are generally used with a full-atom model (although MC techniques can also be applied). In an MD simulation, the position and momentum of every particle, the forces between them, and all external fields must be known at all times. This information is used to simultaneously solve Newton's equations of motion for every particle in the system, to determine its new position and momentum after a very small time step. This procedure is repeated for several million such time steps, usually spanning just a few nanoseconds in real time. The series of particle configurations generated in this way represents a chain of states through which the system passes as it evolves over time. If a suitable set of interaction potentials is available, MD simulations of this type can be extremely useful in providing detailed information about short time-scale properties of the system, even though large-scale movements of the peptide are not observed, and great care must therefore be taken in choosing a starting configuration for the system. To study longer timescale behaviors of biological systems (e.g., protein folding, protein insertion into bilayers), the atomic detail must be simplified, an approach known as coarse graining.

Coarse graining recognizes the fact that many of the details in a full-atom model play little or no part in the behavior of interest, or can be replaced by much simpler terms (although such details may be important for a different property of the system). In this way, a much larger system can be simulated for a considerably longer time. We present one such coarse-grained technique that fits somewhere between analytical theoretical methods, and a full-atom simulation. Unlike these methods, our approach allows us to investigate equilibrium states that are kinetically allowed and thermodynamically stable, and consider longer-timescale mechanistic pathways.

There are also many examples of composite models, which include aspects of both full-atom and coarse-grained techniques. In particular, several models have used coarse-grained (mean-field) bilayers, similar to the one presented here, with a full-atom peptide representation (Biggin and Sansom, 1999).

The conditions that facilitate protein immobilization at the surface, self-assembly into a helix and subsequent insertion into the membrane, are of particular interest in the fields of targeted drug delivery, gene therapy, and disease control. Because these are the particular behaviors we are attempting to understand and predict, it is important for our model peptide to be more sophisticated than the simple hydrophobic block used in many theoretical studies, both in

the way that it moves and folds and in the details of its interaction with the lipid bilayer. As a result, following Milik and Skolnick (1993), our model emphasizes the complex hydrophobic, polar, and hydrogen-bonding interactions between the membrane and the different amino-acid residues of the peptide, as well as the flexibility of the peptide chain. To avoid overcomplicating the model, this added complexity is offset by a simplification of some other characteristics of the membrane. As a result, we have neglected many of the physical membrane effects mentioned earlier (e.g., spontaneous curvature), and any steric effects.

We apply the MC simulation technique to a theoretical model of a peptide/lipid bilayer system, to investigate the insertion behavior of two peptides, Magainin2 and M2 $\delta$ . Magainin2 is an antimicrobial peptide from the skin of the *Xenopus* frog, that binds to cell membranes (Zasloff, 1987), but does not lyse red blood cells (Bechinger et al., 1991). It is predominantly helical in detergent micelles, but unfolded in water (Milik and Skolnick, 1993), and solid-state NMR spectra suggest that it adsorbs to the surface of a bilayer but does not insert (Bechinger et al., 1991). In contrast, M2 $\delta$  readily inserts into lipid bilayer membranes, forming a trans-bilayer helix, and lysing red blood cells (Bechinger et al., 1991; Kersch et al., 1989).

Initial attempts were made to simulate the insertion of these peptides using the models and methods of Milik and Skolnick (1993) and Baumgaertner (1996), but without success. As a result, our model includes the "chain of spheres" peptide proposed by Milik and Skolnick (1993) and a variation of their effective medium bilayer approximation, along with a new set of amino-acid transfer energies derived from the work of Roseman (1988a,b) and Jacobs and White (1989). In recognition of the growing evidence that the tail region has some polar content and is not simply a homogeneous nonpolar phase, we can vary the tail polarity in our model from alkane-like to octanol-like via a single parameter,  $f_q$ , the polarity factor. In addition, we take into account the diminished internal (intramolecular) hydrogen bonding at each end of the helical peptide (Engelman et al., 1986; Roseman, 1988a), which has been neglected in previous coarse-grained membrane/peptide models despite the great effect it can have on insertion behavior. A key feature of our model is that the functions and parameters used to define the membrane (water content, polarity, and hydrophobicity) and its interaction with the peptide (amino-acid transfer energies) were not chosen simply to reproduce the experimental insertion behavior of Magainin2 and M2 $\delta$ . They were instead based on several experimental and theoretical studies of phospholipid membrane structure (Jacobs and White, 1989; Milik and Skolnick, 1993; Griffith et al., 1974; Engelman et al., 1986) and an experimental study of the interaction of a lipid bilayer with a series of tripeptides that solubilized in the head region (Jacobs and White, 1989). By setting up our membrane model in this way, it is not specific to the Magainin2 and M2 $\delta$  studies reported here, but should

be generally applicable to a wide range of other peptides, allowing us to reproduce and predict their insertion behaviors as well.

The peptides Magainin2 and M2 $\delta$ , are similar in many ways, but interact quite differently with a phospholipid membrane. A sophisticated theoretical model is therefore required to reproduce their respective behaviors. However, such a model can do far more than simply reproduce the experimentally observed behavior of each system. It also allows us to follow positional and energetic trajectories of individual amino-acid residues during dynamical processes (e.g., insertion), and collect positional, energetic, and orientational probability distribution data for equilibrated configurations, including metastable states. Therefore, in addition to presenting results that show that our model accurately reproduces the macroscopic behavior of both peptide/membrane systems, we also characterize the stable equilibrium configurations of both peptides (and a metastable equilibrium configuration of M2 $\delta$ ), and briefly describe two distinct insertion mechanisms for M2 $\delta$  and a translocation mechanism for Magainin2. We also present results for the interaction of M2 $\delta$  with bilayers of different thicknesses, highlighting the dramatic differences in system behavior that can result from a small change in membrane thickness.

We believe that this model simulates peptide behavior during adsorption at the surface, self-assembly into an  $\alpha$ -helix, and subsequent insertion (under appropriate conditions) more accurately than previous models. Such a detailed understanding of the membrane/peptide system is the first step toward controlling and improving current processes and materials, and designing totally new ones with specific properties. An equally important aspect of this work is that it greatly enhances our understanding of sequence–structure–function relationships.

## THE SIMULATION MODELS

### The peptide model

The model peptide is essentially the same as that described by Milik and Skolnick (1993), and Baumgaertner (1996). It consists of a linked chain of hard spheres, each representing a peptide residue containing backbone and side-chain elements ( $-\text{NH}-\text{C}_\alpha\text{HR}-\text{COO}-$ ). The  $\alpha$ -carbon ( $\text{C}_\alpha$ ) is located at the center of the sphere, and spheres are linked by 3.8-Å-long virtual bonds. The virtual bonds ensure that the  $\text{C}_\alpha$  atoms are always at their experimentally observed equilibrium separation (the mean distance for proteins in the Brookhaven Protein Database), but have no energetic component, acting only as a constraint on the spatial configuration of the peptide. Van Gunsteren and Karplus (1982) have shown that fixing the virtual bond lengths in this way does not adversely affect the simulation dynamics.

In the model of Gregoret and Cohen (1990), the excluded volume of a residue depends on the size of its side-chain.

Represented by a sphere, the ideal radius varies from  $2.02 \pm 0.25$  Å for Gly to  $2.65 \pm 0.45$  Å for Lys, with a second sphere (His, Phe, Tyr) and third sphere (Trp) added for the aromatic residues. Such a model requires the primary sphere to be centered at the center of mass of the residue, which is actually somewhat removed from the backbone and the  $\text{C}_\alpha$  atom, where our hard spheres are centered. As a result, we are unable to use the residue radii given by Gregoret and Cohen, because they would, in all cases, overlap with adjacent residues along the 3.8-Å virtual bonds. However, because the detailed packing of a peptide is not the focus of our work, we have used the 3.0-Å diameter (1.5-Å radius) spheres proposed by Baumgaertner (1996) to more efficiently study the insertion phenomenon. This choice prohibits unrealistic peptide folding, which could occur with smaller hard spheres or no hard spheres at all, while maintaining the simplicity of the model. Our main concern is that the model is able to reproduce the helical folding of a peptide from a random, extended conformation, under the appropriate conditions. This model has such a capability, due to the internal hydrogen-bonding interactions built into the energy calculations, which we describe in the lipid-bilayer model section.

The total energy of the peptide chain,  $U$ , is the sum of six energy terms,

$$U = U_A + U_T + U_S + U_Q + U_B + U_H. \quad (1)$$

These can be grouped into two different classes; environment-independent terms and environment-dependent terms. There are three environment-independent terms: the angle energy,  $U_A$ ; the torsional energy,  $U_T$ ; and the steric energy,  $U_S$ . Although indirectly affected by the local environment of the peptide, the calculation of these terms requires only the peptide chain conformation (i.e., the relative position of each residue with respect to all the other residues). The calculation is thereafter quite straightforward using Eqs. 2. There are also three environment-dependent terms: the total hydrogen bonding energy,  $U_H$ ; the hydrophobic energy,  $U_B$ ; and the polar (hydrophilic) energy,  $U_Q$ . The calculation of these terms requires the position of each residue with respect to the model lipid and surrounding aqueous phase, as well as the overall conformation of the peptide in the case of  $U_H$ . Because the calculation of these terms is dependent on the details of our modified lipid-bilayer model, they will be discussed in the lipid-bilayer model section.

The simplest of the environment independent terms is  $U_S$ , which is zero when no residues overlap, and positive infinite when any two or more residues overlap:

$$U_S = \sum_{i=1}^{N-1} \sum_{j=2}^N V(r_{ij}), \quad j > i,$$

$$\text{where } V(r_{ij}) = 0 \quad \text{for } r_{ij} > \sigma,$$

$$V(r_{ij}) = \infty \quad \text{for } r_{ij} < \sigma. \quad (2a)$$

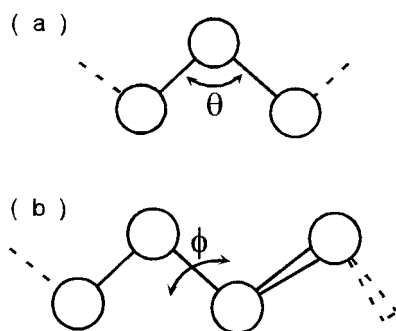


FIGURE 1 (a) The angle between adjacent virtual bonds, and (b) the angle between adjacent planes in the peptide model.

$N$  is the number of residues in the peptide chain,  $r_{ij}$  is the distance between residues  $i$  and  $j$ , and  $\sigma = 3.0 \text{ \AA}$  is the residue hard-sphere diameter. Although listed as an energetic term,  $U_S$  acts more as a spatial constraint on the peptide, ensuring that no configuration contains an overlap.  $U_A$  is a function of angle  $\theta$  (Fig. 1 a), the angle between adjacent virtual bonds:

$$U_A = \sum_{\text{bond angles}} \varepsilon_\theta (\cos \theta - \cos \theta_0)^2, \quad (2b)$$

where  $\varepsilon_\theta = 2.0 \text{ kcal/mol}$  and  $\theta_0 = 89.5^\circ$ .  $U_T$  is a function of angle  $\phi$  (Fig. 1 b), the angle between adjacent planes, each of which is defined by two adjacent virtual bonds,

$$U_T = \sum_{\text{torsional angles}} \varepsilon_\phi [1 - \cos(\phi - \phi_0)], \quad (2c)$$

where  $\varepsilon_\phi = 1.5 \text{ kcal/mol}$  and  $\phi_0 = 52.1^\circ$ . The angle and torsional energy functions have shallow minima at bond and torsional angles of  $89.5^\circ$  and  $52.1^\circ$  respectively, which correspond to the lowest energy (least strained) conformation of the peptide.

### The lipid bilayer model

A lipid bilayer is composed of two opposing lipid monolayers. In an aqueous solution, the hydrophobic acyl chain tails face inward toward the center of the bilayer, and the amphiphilic lipid heads face outward, in contact with the aqueous phase. Our standard bilayer model follows Milik and Skolnick (1993), having a  $4.5\text{-\AA}$ -wide head region at each side and a  $27.0\text{-\AA}$ -wide tail region in the center (i.e.,  $2z_0$ , where  $z_0$  is the length of the acyl chain tail of a single lipid). When a bilayer of a different thickness is modeled,  $z_0$  changes, but the head region remains the same size. Different model bilayers are therefore composed of lipids with similarly sized head groups, but acyl chain tails of different lengths.

Three functions are used to model the head and tail regions of the bilayer, and the surrounding aqueous phase. These functions represent the fractional water content,  $w(z)$ ,

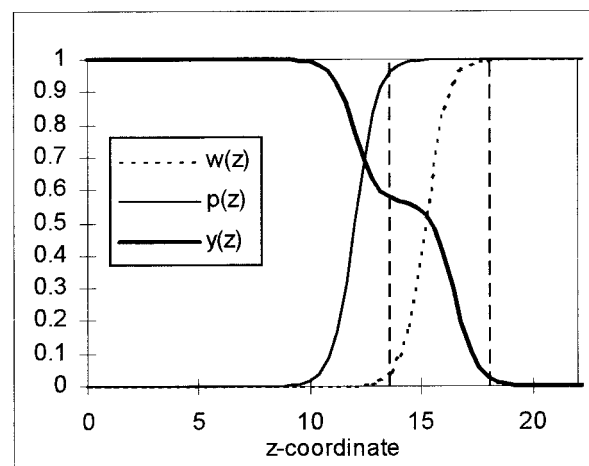


FIGURE 2 The model bilayer functions (symmetrical about  $z = 0$ ). The vertical dashed lines denote the head region.

the polarity,  $p(z)$ , and the hydrophobicity,  $y(z)$ , and are shown in Fig. 2. Each one is a function of the  $z$  coordinate of the system only, where the  $z$  axis is defined perpendicular to the bilayer surface.  $w(z)$  is defined by

$$w(z) = 1 - \left\{ \frac{1}{1 + \exp(w_\lambda [|z| - (z_0 + w_{\text{shift}})])} \right\}, \quad (3)$$

where  $w_\lambda$  defines the shape of the boundary region (where the water content changes from one to zero),  $z_0$  is the length of the acyl chain tail of a single lipid, and  $w_{\text{shift}}$  is the displacement of the boundary center from  $z = z_0$ .  $w(z) = 1$  in the aqueous phase, on either side of the bilayer region, but drops through the head region, reaching zero a short way into the tail region. Although  $w_\lambda = 2$  is used throughout our work (fixing the shape and width of the boundary),  $w_{\text{shift}} = 1.65 \text{ \AA}$  was chosen by fitting simulation data to the experimental data of Jacobs and White (1989) for the adsorption of a series of tripeptides to the surface of a bilayer membrane (see Appendix B). The fitted  $w(z)$  profile matches the observed distribution of water in a lipid bilayer quite well; the amphiphilic head region supports a significant water content, which decreases toward the center of the bilayer, and the outer edges of the hydrophobic tail region contain a small amount of water in the presence of peptide residues (Jacobs and White, 1989).  $w(z)$  is used in conjunction with the peptide conformation to calculate  $U_H$ , the total hydrogen-bonding energy.

Eq. 4 gives the phenomenological helicity factor for a residue pair,  $V_H(r_n)$ , proposed by Milik and Skolnick (1993). It is a function of the measured separation between a residue and its  $n$ th neighbor,  $r_n$ .

$$V_H(r_n) = \frac{1}{1 + [(|r_n| - a_n)/\kappa]^4}, \quad (4)$$

where  $a_n$  is the optimal separation in an  $\alpha$ -helix, and  $\kappa$  is the decay length of the potential. Only the third and fourth



**TABLE 1** Model parameters for twenty common amino acid residues

i	$b_0(i)$	$b_1(i)$	$q_0(i)$	i	$b_0(i)$	$b_1(i)$	$q_0(i)$
Gly (G)	-1.94	0.00	0.00	Glu (E)	-4.10	-1.30	-3.94
Ala (A)	-2.61*	-0.40	0.00	Leu (L)	-4.96*	-0.60	0.00
Ser (S)	-2.86	-0.40	-1.02	Gln (Q)	-4.25	-0.70	-4.43
Cys (C)	-3.93*	-0.50	0.00	His (H)	-4.46	-1.00	-3.61
Pro (P)	-3.23	-0.90	0.00	Met (M)	-4.47	-0.30	-0.87
Thr (T)	-3.36	-0.40	-1.00	Phe (F)	-5.18*	-0.70	0.00
Asp (D)	-3.49	-0.80	-3.12	Lys (K)	-4.97	-0.40	-5.49
Val (V)	-4.12*	-0.40	0.00	Tyr (Y)	-5.21	-1.20	-4.25
Asn (N)	-3.64	-0.90	-3.97	Arg (R)	-5.63	-0.30	-7.58
Ile (I)	-4.96*	-0.40	0.00	Trp (W)	-5.86	-0.60	-1.06

All values are kcal/mol.

\*Value has been adjusted to preclude a positive polar energy.

neighbors along the peptide chain are considered, because these are the main contributors to the internal hydrogen bonding of a given residue (Baumgaertner, 1996), and the parameters  $a_n$  and  $\kappa$  are fixed throughout this work ( $a_{[3]} = 5.04$  Å,  $a_{[4]} = 6.3$  Å; Barlow and Thornton, 1988;  $\kappa = 0.1a_n$ ).  $V_H(r_n)$  is almost a square well potential, with a maximum value of one around the optimal separation decaying rapidly to zero outside this range.  $V_H(r_n)$  is used to calculate  $H_{\text{int}}(i)$ , the internal hydrogen-bonding energy of each residue in the peptide chain,

$$H_{\text{int}}(i) = \frac{H_0}{4} \sum_{n=-4, -3, 3, 4} V_H(r_n), \quad (5a)$$

where  $H_0$  is the maximum hydrogen-bonding energy per residue, including internal (intramolecular) bonding along the peptide backbone and external (intermolecular) bonding with surrounding water molecules.  $H_0 = -6.12$  kcal/mol, which corresponds to the transfer energy of an unbonded peptide group (N—H, O=C), from  $\text{CCl}_4$  to water (Roseman, 1988b). This includes the hydrogen-bonding energy ( $-5.50$  kcal/mol), and the polar interaction energy of the peptide group ( $-0.62$  kcal/mol). We have included the polar interaction energy with the hydrogen-bonding energy because the extent to which both terms contribute to the transfer energy is dependent on the degree of local helicity of the peptide group. A helically folded peptide effectively screens the polar groups of the backbone from the surrounding environment, so there is no energy change on transferring the backbone groups between the aqueous phase and the bilayer. It is therefore appropriate to include the backbone polar interactions in the hydrogen-bonding calculation, rather than with the side chain polar interactions, which are independent of peptide conformation. Our  $H_0$  value is the same one used by Jacobs and White (1989), and Baumgaertner (1996), but different from that used by Milik and Skolnick (1993). Milik and Skolnick used a smaller value ( $-4.1$  kcal/mol), which appears to originate from the work of Klotz and Farnham (1968). However, calorimetric studies later showed the thermodynamic cycle from which

this value was derived to be incorrect (Kresheck and Klotz, 1969). As a result, the corrected transfer energy for an unbonded peptide group, calculated by Roseman (1988b), is  $-6.12$  kcal/mol. For most residues within the peptide chain, the minimum value of  $H_{\text{int}}(i)$  is  $H_0$ , but the last four residues on each end of the chain only have a third and fourth nearest neighbor in one direction along the peptide chain, increasing their minimum  $H_{\text{int}}(i)$  values to  $-4.59$  kcal/mol for the third and fourth residues from the end, and  $-3.06$  kcal/mol for the end two residues. The external hydrogen-bonding energy of each residue,  $H_{\text{ext}}(i)$ , is given by

$$H_{\text{ext}}(i) = w(z_i)[H_0 - H_{\text{int}}(i)]. \quad (5b)$$

This is the energy resulting from hydrogen bonding between the backbone of a residue and the surrounding water molecules.  $w(z)$  accounts for the diminished probability that hydrogen bonds will be formed with water molecules when the surrounding phase has a lower water content. The total hydrogen-bonding energy for a peptide chain,  $U_H$ , is given by

$$U_H = \sum_{i=1}^N [H_{\text{ext}}(i) + H_{\text{int}}(i)]. \quad (6)$$

The polar energy of a residue,  $Q(i)$ , is the interaction energy of the charged and partially charged functional groups of the side chain with the solvent environment,

$$Q(i) = p(z_i)q_0(i), \quad (7)$$

where  $q_0(i)$  is the polar energy of the residue  $i$  side chain in water (Table 1), and  $p(z)$  is the polarity function,

$$p(z) = 1 - \left\{ \frac{f_q}{1 + \exp(p_\lambda[|z| - (z_0 + p_{\text{shift}})])} \right\}, \quad (8)$$

where  $f_q$  is a polarity factor used to select the relative polarity of the tail region,  $p_\lambda$  defines the shape of the boundary region ( $p_\lambda = w_\lambda = 2$ ), and  $p_{\text{shift}}$  is the displacement of the boundary center from  $z = z_0$  ( $p_{\text{shift}} = -1.5$  Å).

The value of  $p_{\text{shift}}$  is chosen so that  $p(z) = 1$  throughout the aqueous phase and amphiphilic bilayer head region, where Jacobs and White (1989) suggest that all polar interactions are satisfied.  $p(z)$  only begins to drop when more than half of the residue has passed into the tail region, reaching its minimum value several Angstroms further into the region, past the small amount of water that gives the tail region some polarity at its outer edges. The total polar energy of the peptide chain,  $U_Q$ , is given by

$$U_Q = \sum_{i=1}^N Q(i). \quad (9)$$

The hydrophobicity function,  $y(z)$ , is given by

$$y(z) = \frac{1 - f_y}{1 + \exp(\gamma_\lambda[|z| - (z_0 + y_{\text{shift1}})])} + \frac{f_y}{1 + \exp(\gamma_\lambda[|z| - (z_0 + y_{\text{shift2}})])}, \quad (10)$$

where  $\gamma_\lambda$  defines the shape of the boundary region ( $\gamma_\lambda = p_\lambda = w_\lambda = 2$ ),  $y_{\text{shift1}}$  and  $y_{\text{shift2}}$  are the displacements of the two boundary centers from  $z = z_0$  ( $y_{\text{shift1}} = -1.5$  Å,  $y_{\text{shift2}} = 3.0$  Å), and  $f_y$  is the fraction of the total hydrophobic energy that is realized when a residue is adsorbed into the head region ( $f_y = 0.56$ ). The values of  $y_{\text{shift2}}$ , and  $f_y$  were chosen to best fit the data of Jacobs and White (1989), whose experimental studies of tripeptide adsorption suggest that ~56% of the available hydrophobic energy is associated with adsorption into the head region, and that adsorbed (but not inserted) residues reside primarily at the headgroup midplane (see Appendix B).  $y_{\text{shift1}}$  was chosen to yield the remaining hydrophobic energy as the residue passes into the tail region.  $y(z) = 0$  throughout the aqueous phase, and  $y(z) = 1$  for most of the tail region.

$y(z)$  is used to calculate  $B(z_i)$ , the hydrophobic energy of a peptide residue at any point along the  $z$  axis:

$$B(z_i) = y(z_i)b_0(i) + b_{\text{hlx}}(i)[1 - y(z_i)], \quad (11a)$$

where  $b_0(i)$  is the water-to-alkane hydrophobic Gibbs transfer energy of residue  $i$  (Table 1), and  $b_{\text{hlx}}(i)$  is the side-chain hydrophobic energy change of residue  $i$  due to the peptide conformation in the aqueous phase.  $b_0(i)$  is calculated from  $A_a(i)$ , the stochastic accessible surface area of a residue (Table 4 of Jacobs and White, 1989; Rose et al., 1985), and  $C_s$ , the solvation coefficient for an alkane solvent ( $C_s = -22$  cal/mol Å<sup>2</sup>; Richards, 1977) as shown in

$$b_0(i) = C_s A_a(i) \quad (11b)$$

(Reynolds et al., 1974).  $b_{\text{hlx}}(i)$  derives from the loss of accessible surface area when the peptide chain has some degree of local helicity,

$$b_{\text{hlx}}(i) = \frac{b_1(i)}{4} \sum_{n=-4, -3, 3, 4} V_H(r_n), \quad (11c)$$

where  $b_1(i)$  is the maximum reduction in hydrophobic energy due to helical folding (Table 4 of Roseman, 1988a) (Table 1), and  $V_H(r_n)$  is the helicity factor of Eq. 5a.  $U_B$  is the total hydrophobic energy of the peptide chain,

$$U_B = \sum_{i=1}^N B(i). \quad (12)$$

It should be noted that, in general, entropy terms are omitted from energy summations used in computer simulations because the simulation method itself incorporates entropic effects—less likely configurations of the system will be sampled less often. Only the enthalpy (or internal energy, depending on the ensemble) needs to be considered explicitly. However, the energy change that accompanies the transfer of a hydrophobic group from water to a nonpolar solvent (the hydrophobic effect) is due almost entirely to an entropy change, the enthalpy change being negligible (Jacobs and White, 1989; Jain et al., 1985). Because our model has a simplified peptide representation and no water molecules, the local ordering of water around hydrophobic groups, which causes the hydrophobic effect, cannot occur. The simulation will therefore not implicitly account for the entropy associated with water structuring, which must be included in the hydrophobic energy term (this energy term thus becomes a Gibbs energy term), as in any analytical solution. Here, we have avoided the problem of calculating the transfer enthalpies and entropies separately by using empirical Gibbs transfer energies (via  $C_s$  and  $A_a$ ). Other entropic effects, related to the peptide conformation and localization in the bilayer, do not need to be considered explicitly, because they are accounted for by the simulation procedure, even for our simplified peptide model.

### The model parameter set

Because there are almost as many residue/bilayer parameter sets as there are models, each one working to the satisfaction of its creators but not widely used elsewhere, there was no clear choice for our work (for a good review, see Engelman et al., 1986). As a result, we have created a new parameter set from reliable primary data taken from experimental and theoretical sources. This parameter set was generated independent of the simulation results, with no parameter fitting. Because it is not tied to any specific peptide/bilayer system, it can be applied equally well to a wide range of systems.

The parameter set (Table 1) consists of three residue-specific values, the water-to-alkane Gibbs transfer energy (hydrophobic energy),  $b_0(i)$ ; the side-chain polar energy in the aqueous phase,  $q_0(i)$ ; and the hydrophobic energy change due to local helicity,  $b_1(i)$ . The  $b_0(i)$  values are calculated via Eq. 11b, and include the hydrophobic energy of the residue backbone,  $b_0(\text{bb}_i)$ , and residue side-chain,

$b_0(\text{sc}_i)$ . Because all residues have the same backbone structure, and glycine has no side-chain, the backbone hydrophobic energy of every residue is equal to the total hydrophobic energy of glycine,  $b_0(\text{bb}_i) = b_0(\text{glycine}) = -1.94$  kcal/mol. Therefore, the side-chain hydrophobic energy for each residue can easily be found:

$$b_0(\text{sc}_i) = b_0(i) - b_0(\text{bb}_i). \quad (13)$$

The side-chain hydropathies of Table 3 of Roseman (1988a), corrected for self-solvation, are sums of the polar and hydrophobic energies for water-to-alkane transfer of the residue side-chains at pH 7.0,  $q_0(\text{sc}_i) + b_0(\text{sc}_i)$ . Subtraction of  $b_0(\text{sc}_i)$ , calculated in Eq. 13, yields  $q_0(\text{sc}_i)$ . Because the polar interaction energy of the residue backbone,  $q_0(\text{bb}_i)$  (i.e., the peptide group described earlier), is small and included in the hydrogen bonding energy,  $q_0(i)$  is just the side-chain polar energy,  $q_0(\text{sc}_i)$ , which must either be zero for nonpolar groups, or negative for polar groups. A positive value would erroneously infer that a polar group prefers a nonpolar environment to water. However, the method outlined above produces a slightly positive polar energy (ranging from 0.01 to 0.98 kcal/mol) for six residues, and, so, a small correction is applied to  $b_0(\text{sc}_i)$  for these residues, which reduces  $q_0(i)$  to zero. These corrections to  $b_0(i)$  are noted in Table 1. The  $q_0(i)$  values for some of the polar residues may not appear to be negative enough at first glance. Indeed, simple theoretical estimates and partitioning studies conducted using individual amino acids both suggest that the polar transfer energies should be more positive ( $q_0(i)$  more negative) than those presented here. However, Roseman (1988a) shows that such estimates are invalid for amino acids within a peptide chain, and that a variety of effects, including self-solvation, reduce the effective charges on the side chains. As a result, the insertion of polar residues within a peptide chain is actually considerably easier than early studies suggested. Our  $q_0(i)$  transfer energies take these charge-reducing effects into account, and are therefore the appropriate values to use for the transfer of residues within a peptide chain. Finally, the  $b_1(i)$  values in Table 1 come directly from Table 4 of Roseman (1988a).

Although the  $q_0(i)$  parameters given in Table 1 are independent of the bilayer structure, the polarity function,  $p(z)$ , is dependent on the polarity of the bilayer tail region. The tail region is not simply a homogeneous solvent, but rather a complex tangle of acyl chains, cavities, and a small number of water molecules, giving it characteristics of both octanol and hexadecane-type solvents (Roseman, 1988a). The electron spin resonance studies of Griffith et al. (1974) even suggest a gradient of polarity from the center of the tail region, which is hexane-like, to the edge of the tail region, which is more octanol-like (the arguments made by a number of investigators in favor of an octanol-like or alkane-like tail region are reviewed by Stein (1986)). Our polarity function, Eq. 8, therefore includes a polarity factor,  $f_q$ ,

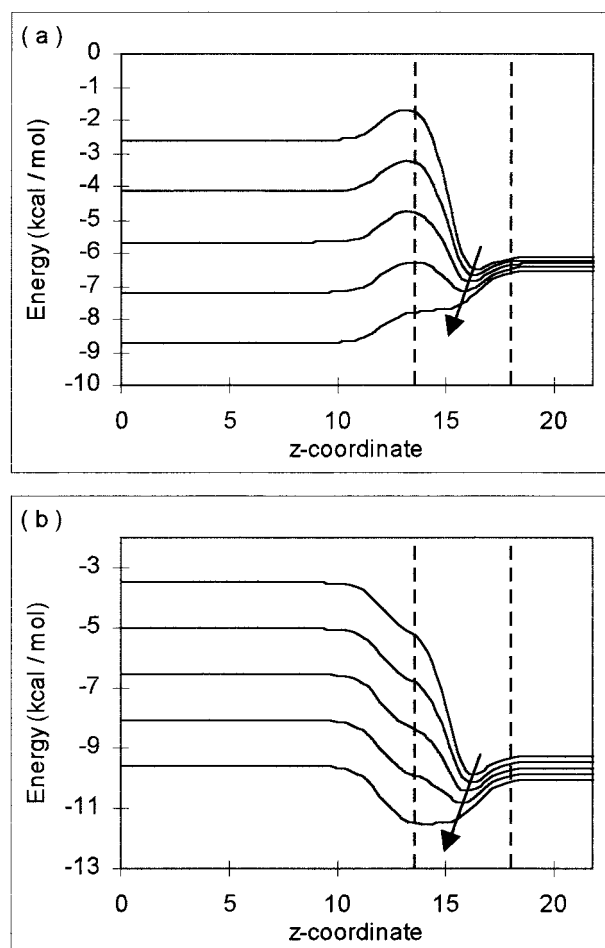


FIGURE 3 Total energy functions (symmetrical about  $z = 0$ ) for a range of local helicities, for (a) alanine and (b) aspartine. Local helicities shown are (from the top), 0%, 25%, 50%, 75%, and 100%. Vertical dashed lines denote the head region.

which allows us to vary the polarity of the bilayer tail region to model all types of bilayer tail polarity. The polarity factor modifies the polar energy of each residue,  $Q(i)$ , as it enters the tail region, via  $p(z)$  in Eq. 7. If the bilayer tail region is assumed to be alkane-like,  $f_q = 1.00$ , and if it is octanol-like,  $f_q = 0.65$  (the water-to-octanol transfer energies for polar residues given by Jacobs and White (1989) average around 65% of the corresponding water-to-alkane values). We can also investigate bilayers with intermediate polarity tail regions, for which  $0.65 \leq f_q \leq 1.00$ .

The sum totals of the environment-dependent residue energies,  $H(i)$ ,  $Q(i)$ , and  $B(i)$ , at different local helicities, are shown in Fig. 3, a and b, for alanine and aspartine, respectively. Alanine is a nonpolar residue, and aspartine is a strongly polar residue (an alkane-like tail region is assumed in each figure). In each figure, the top curve represents zero local helicity ( $V_H = 0$ ), whereas the bottom curve represents the completely helical case ( $V_H = 1$ ). For both residues, a small energy well close to the middle of the head region

enables all residues to adsorb to the bilayer when the local helicity is zero. However, a large energy barrier makes insertion into the tail region unlikely for locally nonhelical residues. This barrier is primarily due to the loss of external hydrogen bonds, with an additional loss of polar interactions increasing the barrier height in the case of aspartine. In contrast, there is a dramatic change in the total energy curve when the residues have complete local helicity. In this case, the hydrogen bonding is entirely internal, and therefore indifferent to the water content. The alanine curve now has no barrier to insertion into the tail region, and the aspartine barrier is much smaller. The arrows in the figures illustrate the energetic driving force for helical self-assembly in the head region. After adsorption into the head region, a large energy barrier prevents the further progress of a nonhelical peptide into the tail region, but an increase in local helicity allows each residue to attain a lower energy state. Random conformational fluctuations in the peptide chain that result in greater helicity will therefore be favored. Given a high enough degree of local helicity, the nonpolar residues can spontaneously insert into the tail region, though the strongly polar residues may still be prevented from doing so by the residual energy barrier. So, although all residues favor adsorption and helical self-assembly within the head region of the model bilayer, the balance between polar and nonpolar residues (i.e., their energies and also their position within the peptide chain) will dictate which peptides insert into the tail region, and which do not.

Magainin2 and M2 $\delta$  are 23-residue amphiphilic membrane peptides that interact quite differently with lipid bilayers (Bechinger et al., 1991). Magainin2 has the sequence

**GIGKFLHSAKKFGKAFVGEIMNS**,

and M2 $\delta$  has the sequence

**EKMSTAI SVLLAQAVFLLLSQR**.

Residues with no side chain (G) or a nonpolar side chain ( $q_0 = 0$  kcal/mol) are shown in bold typeface, and those with a polar side chain ( $q_0 < 0$  kcal/mol) are shown in regular typeface. The N-terminus is to the left of the sequence in each case. All the parameters used to model the different residues are given in Table 1.

## THE SIMULATION METHOD

The canonical MC simulation method is used throughout this work (Allen and Tyllesley, 1989), the canonical ensemble being the appropriate choice for our system, in which the volume, temperature, and number of particles remain constant. In a closed system such as this, internal energy and Helmholtz free energy are considered instead of the more familiar enthalpy and Gibbs free energy terms of open systems. However, because the volume change accompanying real peptide adsorption and insertion into a membrane is negligible, the closed and open system terms are

equal and interchangeable in this case. Periodic boundary conditions are applied in all directions of the three-dimensional simulation box, so that a particle exiting the box in any direction will reappear at the opposite side. Given a sufficiently large box (at least twice the length of the longest interaction potential between particles), periodic boundaries adequately represent infinite space for a model system. As usual, the minimum image convention for particle interactions is used in conjunction with the periodic boundaries. In this convention, interactions are calculated from the minimum separation between two particles, which may be measured across the simulation box, or across a periodic boundary. Appendix A describes how the chain of system configurations integral to the MC method is generated in our simulations.

MC simulations are most commonly used when the number of particles within the system fluctuates (e.g., in the grand canonical or Gibbs' ensembles). In such cases, the chain of system configurations exists "out of time"—a configuration is not necessarily related in time to the previous or next configuration. This is largely because particles may be created within, or deleted from, the system (more accurately, these particles are transferred between the simulated portion of the real system, and somewhere outside the simulated region). In reality, it would take an unknown amount of time for such a configurational change to occur, if such a change was even possible (energetic or physical barriers may rule out altogether the large-scale movement associated with a creation or deletion). So, although the chain of configurations correctly samples phase space giving good ensemble averages, it yields no time-dependent information. In confined systems such as ours, where the particles move around but are never created or deleted from the system, the situation is slightly different. The exact time between successive configurations is still unknown for MC simulations in the canonical ensemble, preventing the calculation of time-dependent properties such as the diffusion coefficient, but successive configurations are much more closely related. If the configurational perturbations are sufficiently small, then it is unlikely that energetic or physical barriers will be bypassed between configurations, and the chain of states can be said to approximate a time-independent relaxation of the system. This means that, as well as enabling us to measure equilibrium properties of the system, we can also examine the relaxation pathway, i.e., the mechanism by which the system changes from its initial state to its equilibrated state.

Unless otherwise indicated, the system temperature was 305 K for all simulations, which is above the thermal phase transition of the lipid membrane. Each simulation run consisted of 50 million MC steps, and took  $\sim 4$  h to run on a Microway Screamer-LX SuperCache-8 workstation with a 667 MHz DEC Alpha 21164 CPU (Microway, Kingston, MA). Because each MC step consists of three configurational changes, 150 million configurations were sampled



**TABLE 2** Percentage of simulation runs in which the final peptide configuration is a trans-bilayer helix

$f_q$	Magainin2 initial configuration		M2δ initial configuration	
	Aq. phase	Trans- bilayer	Aq. phase	Trans- bilayer
0.65	0 (5)	20 (5)	80 (5)	100 (5)
0.70	—	—	40 (10)	100 (2)
0.75	—	—	50 (10)	100 (2)
0.80	—	—	20 (10)	100 (2)
0.85	0 (5)	0 (5)	10 (10)	100 (2)
0.90	—	—	10 (10)	100 (2)
1.00	0 (5)	0 (5)	0 (10)	100 (2)

The total number of runs is shown in parenthesis.

during each simulation. The initial configuration was either an aqueous phase random coil, or a trans-bilayer helix. The random coil configuration was generated by a 50,000-step MC simulation of a peptide in the aqueous phase, using a lattice-type peptide structure as the starting configuration. The internal hydrogen bonding energy of the peptide was monitored to ensure that all memory of the lattice-type structure was lost by the end of the simulation. After  $\sim 10,000$  steps, the internal hydrogen-bonding energy had decreased from an initial value of zero to its final equilibrium value (due to thermal fluctuations, this is actually an equilibrium range). A further 40,000 steps, in which the internal hydrogen bonding energy remained within the equilibrium range, ensured that the peptide was fully equilibrated to an aqueous random coil conformation. For its use in bilayer simulations, this random peptide conformation is shifted laterally, so that it is located entirely within the aqueous phase of the system, and has no initial interaction with the lipid bilayer. The other initial peptide conformation used here is a trans-bilayer helix, which was generated from the random conformation via a 50-million-step simulation using conditions favorable to insertion.

## RESULTS AND DISCUSSION

The qualitative insertion behavior of our model peptides is summarized in Table 2. We investigated a range of membrane tail polarities, indicated by the polarity factor,  $f_q$ , from octanol-like ( $f_q = 0.65$ ) to alkane-like ( $f_q = 1.00$ ). Aqueous phase and helical trans-bilayer initial configurations were used in each case. The results represent the percentage of runs for which a trans-bilayer helix was the final system configuration, with the number of runs indicated in parentheses.

Starting from a random, aqueous phase configuration, Magainin2 very rapidly adsorbs to the bilayer surface, and assembles into a loose helical structure within the head region. It can move laterally within this region and can translocate through the membrane at  $f_q = 0.65$ , but never

irreversibly forms a trans-bilayer helix. Starting from a trans-bilayer helix, Magainin2 remains in that conformation in one out of five simulations at  $f_q = 0.65$ , and in no simulations at higher  $f_q$ . These results show that the equilibrium configuration for Magainin2 in our model bilayer (at all polarities) is a loose helix, adsorbed in the head region. The results from random initial configurations alone do not discount the possibility that Magainin2 could eventually insert, given a long enough simulation run. However, the instability of the trans-bilayer conformation suggests that the barrier preventing Magainin2 insertion is thermodynamic, rather than kinetic. Although the trans-bilayer conformation has a lower internal energy,  $U$ , than the adsorbed conformation, it has a higher Gibbs energy at 305 K (the simulation implicitly includes the system entropy and thus generates an equilibrium configuration in which the Gibbs energy, rather than the internal energy,  $U$ , is minimized). Therefore, even when it is initially a trans-bilayer helix, Magainin2 will not remain in this thermodynamically unstable state for long. The only exception was at  $f_q = 0.65$ , for which the Gibbs energy difference between the trans-bilayer and adsorbed conformations is smallest. Although still unlikely, it is possible for the metastable trans-bilayer conformation to survive for the duration of a 50-million-step simulation in a bilayer of this type. At very low temperatures, the entropy difference is negligible, and the internal energy,  $U$ , becomes the deciding thermodynamic factor. Under these conditions, Magainin2 should therefore be more stable in the trans-bilayer conformation than in the head region. This hypothesis was confirmed by a simulation at 50 K and  $f_q = 1.00$ , in which trans-bilayer Magainin2 remained in the trans-bilayer conformation throughout a 50-million-step run. It should be noted however, that our model bilayer bears no relation to a real bilayer at 50 K, and the only purpose of this low-temperature simulation was to confirm the entropic contribution to the equilibrium state of Magainin2 at 305 K.

The behavior of M2δ is quite different. This peptide also rapidly adsorbs to the lipid bilayer from its initially random, aqueous phase structure, forming a loose helix in the head region. However, for all but the nonpolar, alkane-like bilayer ( $f_q = 1.00$ ), M2δ inserts and forms a trans-bilayer helix in at least one simulation run. When the peptide inserts, the trans-bilayer form remains stable for the remainder of the simulation. In addition, when the initial configuration is a trans-bilayer helix, the peptide remains in this configuration throughout the simulation. For M2δ, the helical trans-bilayer form is the thermodynamically stable structure, having the lowest Gibbs energy and the lowest internal energy,  $U$ . Only kinetic factors prevent M2δ from inserting from the aqueous phase in every simulation. For each bilayer with tail polarity,  $f_q \leq 0.90$ , insertion occurs in at least one simulation, proving that the kinetic barrier to insertion is not insurmountable, given enough time. Only the bilayer with alkane-like tail polarity ( $f_q = 1.00$ ) resists

peptide insertion in every simulation. The kinetic barrier to insertion may be insurmountable for this bilayer at 305 K, or insertion may simply require longer simulations. The reduction in insertion percentage as the tail polarity decreases ( $f_q$  increases) suggests that the size of the kinetic barrier is inversely proportional to tail polarity. This is to be expected because the energy of each inserted polar residue is also inversely proportional to tail polarity. A decrease in tail polarity, therefore, results in higher energy intermediate species and a reduction in the percentage of simulations in which insertion is observed.

We have successfully reproduced the experimental behavior of Magainin2 and M2 $\delta$  in lipid bilayers for a range of tail polarities (the insertion of M2 $\delta$  is not directly observed for  $f_q = 1.00$ , but a trans-bilayer helix is shown to be the thermodynamically preferred form, and the possibility of insertion cannot be discounted for a very long simulation run). The success of our model, regardless of tail polarity (within the given range), prevents us from recommending a single  $f_q$  value for all bilayer simulations. However,  $f_q = 0.85$  comes closest to the suggestions of Roseman (1988a) and Griffith et al. (1974), that the tail region polarity is somewhere between that of octanol and hexadecane. The following discussion of equilibrium properties will therefore concentrate on peptide behavior in this bilayer model.

An advantage of simulation over experiment is the relative ease with which the microscopic details of a system can be observed. A model that accurately reproduces the macroscopic behavior of a system can also provide a wealth of information at the molecular level. We are therefore able to examine the equilibrium structures of adsorbed Magainin2, adsorbed M2 $\delta$  (metastable state), and inserted M2 $\delta$  in great detail. The results in Table 2 consider the final peptide configuration of each simulation, which tells us whether the peptide inserted or merely adsorbed to the surface. In contrast, equilibrium properties require the sampling of configurational data throughout the simulation. Equilibrium properties are often presented as average values, with no information given about the data spread, but this can be extremely misleading for non-Gaussian data (i.e., data points are not symmetrically distributed about the mean). Here, we consider the probability distribution of chosen properties instead. For the three peptide configurations, Fig. 4 shows probability distribution curves for peptide length, and Fig. 5 shows probability distribution curves for peptide tilt. Length is defined as the separation of end residues, and tilt is defined as the angle  $\alpha$ , between a line connecting the end residues, and the  $z$  axis. In all cases,  $0^\circ \leq \alpha \leq 180^\circ$ , and when the N-terminus inserts before the C-terminus,  $\alpha > 90^\circ$ . The difference between inserted and adsorbed species is very clear, even though the probability distribution curves are not identical for the two adsorbed species. The average length of inserted M2 $\delta$  is 33 Å, and the fluctuation in length is minimal. This corresponds to a perfect  $\alpha$ -helix, which is fairly rigid, and has average distance between residues of

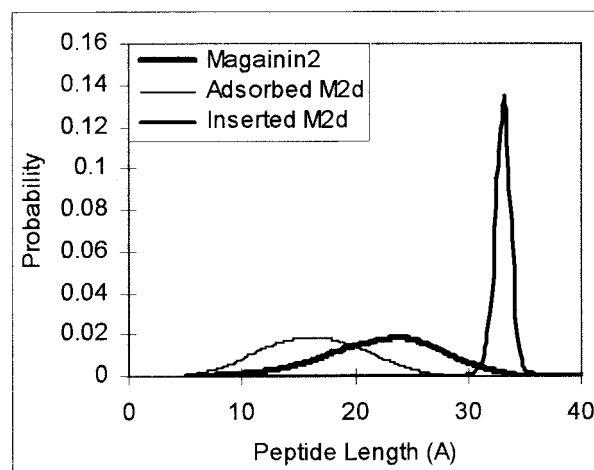


FIGURE 4 Peptide length distribution functions for Magainin2, adsorbed M2 $\delta$ , and inserted M2 $\delta$ .

1.5 Å (Baumgaertner, 1996). In contrast, the adsorbed conformations have a smaller average length (16 and 23 Å), and a much wider distribution, indicating a bent equilibrium state and greater flexibility. The tilt angles of adsorbed and inserted species are similarly distinct. The adsorbed peptides lie in the bilayer surface, perpendicular to the  $z$  axis, indicated by a peak in the probability distribution function at a tilt of  $90^\circ$ . The slight shoulders in these curves indicate very closely related equilibrium variants in which the N-terminus of Magainin2, and the C-terminus of M2 $\delta$  dip slightly into the bilayer. In contrast, the probability distribution function for inserted M2 $\delta$  peaks at  $165^\circ$ , which is almost parallel to the  $z$  axis and indicative of a trans-bilayer configuration. The peak width indicates fluctuations in the tilt angle for all species, illustrating the dynamic nature of the equilibrium configurations.

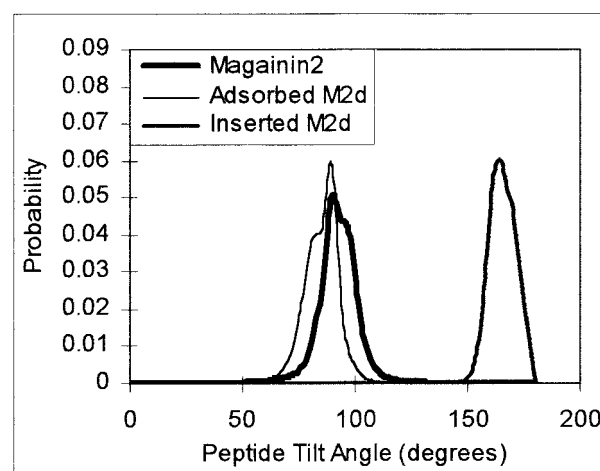


FIGURE 5 Peptide tilt angle distribution functions for Magainin2, adsorbed M2 $\delta$ , and inserted M2 $\delta$ .

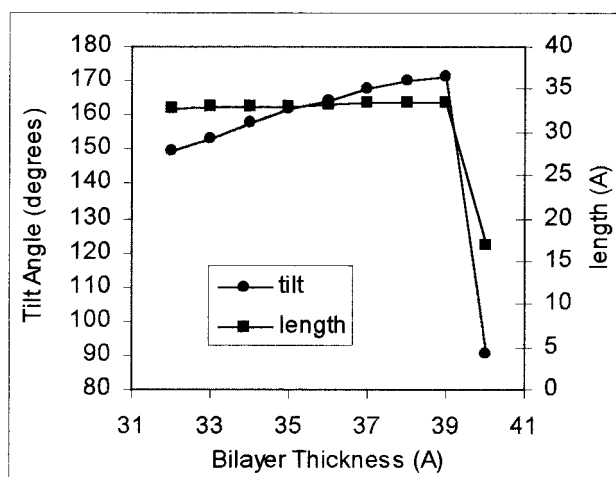


FIGURE 6 M2 $\delta$  length and tilt angle as a function of lipid bilayer thickness.

Although inserted M2 $\delta$  was initially expected to lie along the  $z$  axis, rather than  $15^\circ$  short of parallel, a series of simulations using different bilayer thicknesses provided an explanation. Figure 6 shows the peak values from the length and tilt probability distribution functions for bilayers of different thickness. The standard thickness used here and elsewhere is 36 Å (Milik and Skolnick, 1993, 1995; Baumgaertner, 1996). Although the peptide length remains constant, the tilt angle is a function of the bilayer thickness. Because the most stable peptide configuration is a perfect helix with its terminal residues at the center of each head region, it assumes this configuration whenever possible. In thinner bilayers, the 33-Å-long helix tends to tilt away from the  $z$  axis to accommodate the preferred configuration, rather than compressing or bending to remain parallel to the axis. The thinner the bilayer, the greater the tilt. For thicker bilayers, there is a maximum thickness for which inserted M2 $\delta$  is more stable than adsorbed M2 $\delta$ . This occurs at 39 Å for our model. At 40 Å and beyond, the peptide can no longer span the bilayer while maintaining its preferred helical structure, and rapidly assumes the adsorbed configuration, eschewing any intermediate, partially inserted form. This configurational preference is indicated by the sudden change in tilt angle (to  $90^\circ$ ) and peptide length (to 17 Å). It should be noted that, although the thickness of our bilayer model is rigidly fixed, the tails of a real bilayer are quite flexible, allowing it to stretch or compress in the  $z$  direction, to better accommodate a trans-bilayer peptide. Perturbations of this kind increase the energy of the bilayer, but may decrease the energy of the system by stabilizing the lower energy trans-bilayer configuration of the peptide (Dan and Safran, 1995). However, this type of local thinning or thickening of the bilayer around an inserted peptide is beyond the scope of our current model.

Figures 7 *a*, 8 *a*, and 9 *a* show the equilibrium  $z$  coordinates of all residues in adsorbed Magainin2, adsorbed M2 $\delta$ ,

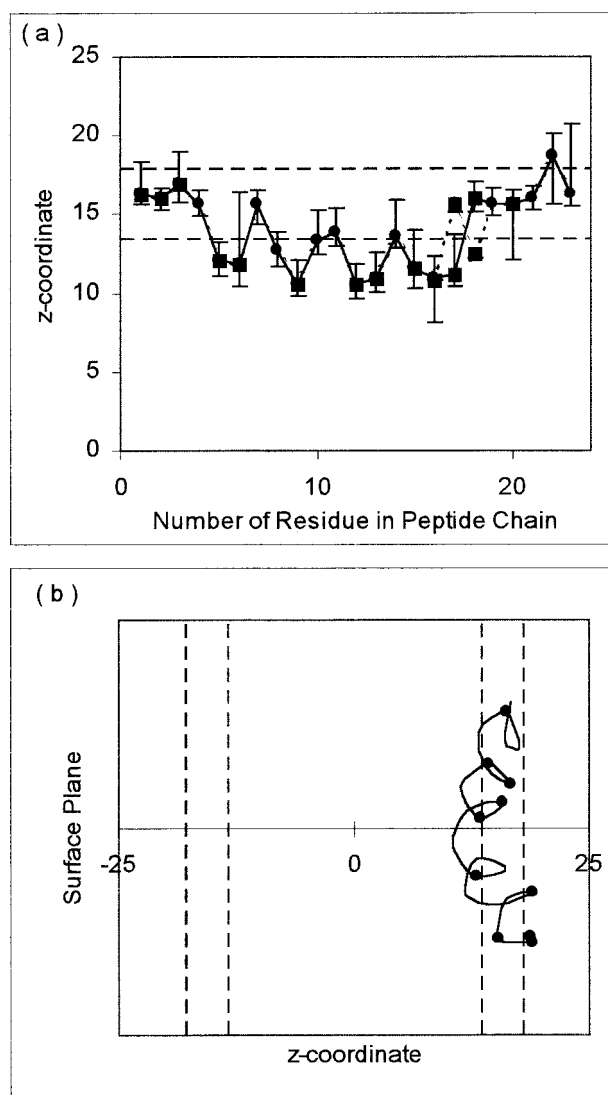


FIGURE 7 Magainin2. (a) residue  $z$ -coordinate ranges, and (b) a representative equilibrium configuration. Squares denote nonpolar residues, circles denote polar residues. Dashed lines indicate the head region.

and inserted M2 $\delta$ , respectively. Milik and Skolnick (1993), and Baumgaertner (1996) show similar plots, but their  $z$  coordinates are simple simulation averages. As noted above, averages omit useful information, and can sometimes be quite misleading. Instead, we generated probability distribution plots for the  $z$  coordinate of each residue, and used these data to produce the equilibrium  $z$ -coordinate ranges of these figures. As expected, no residue had a fixed  $z$  coordinate, but many had extremely broad, and usually asymmetrical probability distributions. Furthermore, some distributions contained more than one peak, indicating multiple locally stable residue locations. The circles and squares therefore represent the  $z$  coordinate of the highest peak in the probability distribution (the most likely  $z$  coordinate), and the error bars represent the  $z$ -coordinate range at half

the main peak height. Multiple peaks were only plotted separately when the valley height between them dropped below half the main peak height. In these cases, the alternate, lower peak position is indicated with a dotted line. Residues with polar side chains ( $q_0 < 0$ ) are shown as circles, and entirely hydrophobic residues are shown as squares.

The equilibrium  $z$  coordinates of Magainin2 (Fig. 7 *a*) illustrate several phenomena; first, the four terminal residues at each end prefer to remain in the head region, even though one end is substantially hydrophobic in character. These residues are unable to satisfy all of their hydrogen-bonding requirements internally, and the presence of water molecules in the head region allows some external hydrogen bonding to occur. Second, wherever possible, the polar residues prefer to remain outside, or at the outer edge of the tail region. This is due to the energy increase experienced by a polar residue on entering the tail region, where it can no longer form strong polar interactions. Finally, although some residues are relatively fixed in the  $z$  direction, having a small  $z$ -coordinate range, others are quite mobile, with an equilibrium range of several Angstroms. In two cases, the residue has dual peaks, showing that it can occupy two essentially separate positions, "snapping" from one position to the other, but spending little time in between. For Magainin2, the distribution of polar residues throughout the peptide serves to anchor its middle section on the edge of the tail region, while the external hydrogen bonding interactions keep its ends in the midst of the head region. Figure 7 *b* shows a representative Magainin2 equilibrium configuration. Although the peptide spends most of its time in this type of conformation, large fluctuations can occur, and any part of the peptide can insert under the right conditions. Indeed, when the bilayer tail region is most accommodating ( $f_q = 0.65$ ), the peptide is able to pass entirely through the bilayer, reforming its equilibrium structure in the opposite head region. This process, known as translocation, occurred in 40% of our simulations involving octanol-like bilayer tails, and is described in more detail below.

The general orientation of Magainin2 and its position in the head region are in agreement with the experimental results of Bechinger et al. (1991), and the simulations of Milik and Skolnick (1993). However, the deeper insertion of the central section of our model peptide, relative to its ends, is the opposite of the Milik and Skolnick predicted conformation. This is due to the incomplete hydrogen bonding of inserted end residues in our model, and, although a minor feature here, such a difference could be fundamental to the behavior of this and other peptides in different circumstances (note: the results of Bechinger et al. do not contain enough detail to confirm either conformation).

Figure 8 *a* shows the equilibrium  $z$  coordinates of the adsorbed M2 $\delta$  conformation. This is a metastable equilibrium state, which shows long-term stability in many of our simulations. It is useful to examine this metastable state to

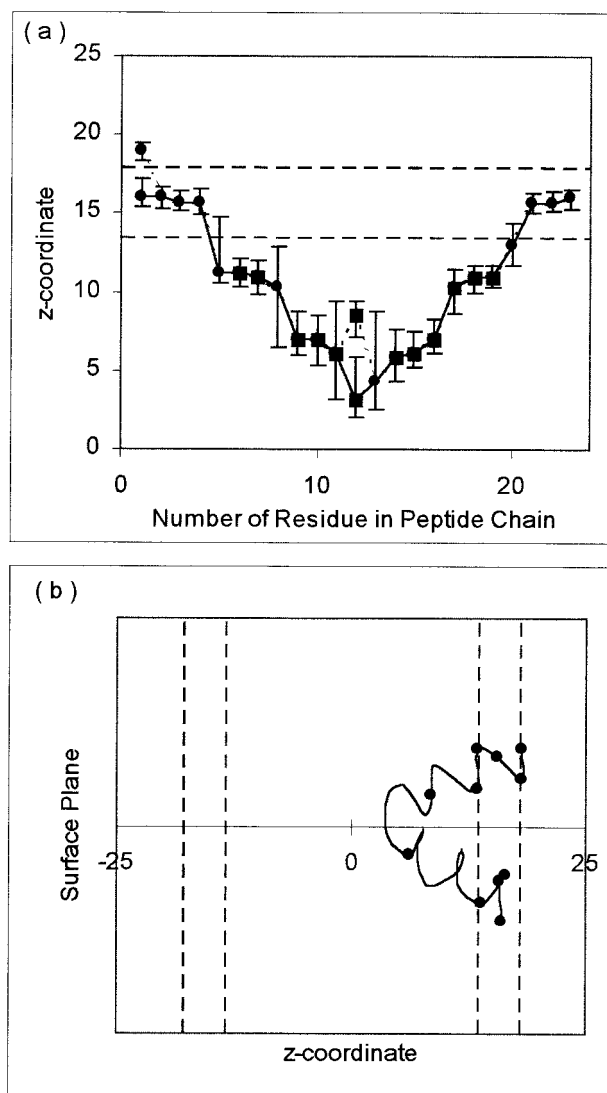


FIGURE 8 Adsorbed M2 $\delta$ . (a) residue  $z$ -coordinate ranges, and (b) a representative equilibrium configuration. Squares denote nonpolar residues, circles denote polar residues. Dashed lines indicate the head region.

understand the reasons for its stability, and the factors that prevent this conformation from inserting. Although M2 $\delta$  contains a comparable number of polar residues to Magainin2, they are distributed quite differently, being concentrated at the ends of the peptide, rather than evenly spread along the whole chain. The end residues are considerably more stable in the head region of the bilayer than the tail region, due to their polar side chains and reduced internal hydrogen-bonding capabilities. In contrast, the middle section of the peptide is extremely hydrophobic, containing only two residues with polar side chains, and has a lower energy within the tail region of the bilayer. These preferences are optimized in the metastable equilibrium structure, in which the ends remain in the head region, while the middle section extends up to 10 Å into the tail region. To



accommodate the surrounding hydrophobic residues, the two centrally located polar residues are also dragged into the tail region at some small energy cost. As a result of this u-shaped conformation, the ends of the peptide are brought closer together, reducing the average length of the peptide, as defined above. Adsorbed M2 $\delta$  is therefore significantly shorter than adsorbed Magainin2, as seen in Fig. 4, though both have very broad length distributions, indicating a high degree of flexibility. Figure 8 *b* shows a representative equilibrium configuration of adsorbed M2 $\delta$ . Like Magainin2, the adsorbed form of M2 $\delta$  shows a good deal of helicity. This metastable conformation for M2 $\delta$  has not been described elsewhere, although its conformational type, dubbed a “helical hairpin” has been characterized by Engelman and Steitz (1981), and modeled by Baumgaertner (1996).

Figure 9 *a* shows the equilibrium *z* coordinates of M2 $\delta$  after insertion. Inserted M2 $\delta$  forms a fairly rigid  $\alpha$ -helical conformation that spans the bilayer from head region to head region. The reduced flexibility of this structure leads to narrower *z*-coordinate ranges for most of the residues. The exceptions are those residues on the border between the head and tail regions, which tend to be at either side of the polar energy slope, rather than on the slope itself. Figure 9 *b* shows a representative equilibrium configuration of inserted M2 $\delta$ , illustrating its straight, helical nature, and also its average tilt angle with respect to the *z* axis. This predicted conformation of M2 $\delta$  is in close agreement with the model of Milik and Skolnick (1993), and the experimental results of Bechinger et al. (1991).

### M2 $\delta$ insertion mechanisms

Two different mechanisms have been identified for the M2 $\delta$  insertion process, referred to as type I and type II. Figure 10 shows a series of simulation snapshots taken during a type I insertion (at  $f_q = 0.65$ ), and Fig. 11 shows a series of snapshots taken during a type II insertion (at  $f_q = 0.85$ ).

Type I insertion begins with the normal adsorbed M2 $\delta$  structure (Fig. 10 *a*). The peptide first rotates one end into the tail region, without significantly altering its conformation (Fig. 10 *b*), then gradually straightens (Fig. 10 *c*). In this fully extended state, the inserted end can move freely until it locates the head region and forms a trans-bilayer helix (Fig. 10 *d*). This is reminiscent of the helical hairpin insertion mechanism postulated by Engelman and Steitz (1981).

Type II insertion is initiated by the formation of an intermediate species (Fig. 11 *a*) from the normal adsorbed M2 $\delta$  structure. The intermediate forms when the center section of the peptide migrates to the edge of the head region. This creates a straight helical segment along the bilayer head/tail interface, relative to which both ends of the peptide are misaligned. The first step is a realignment and partial insertion of one end of the peptide (Fig. 11 *b*).

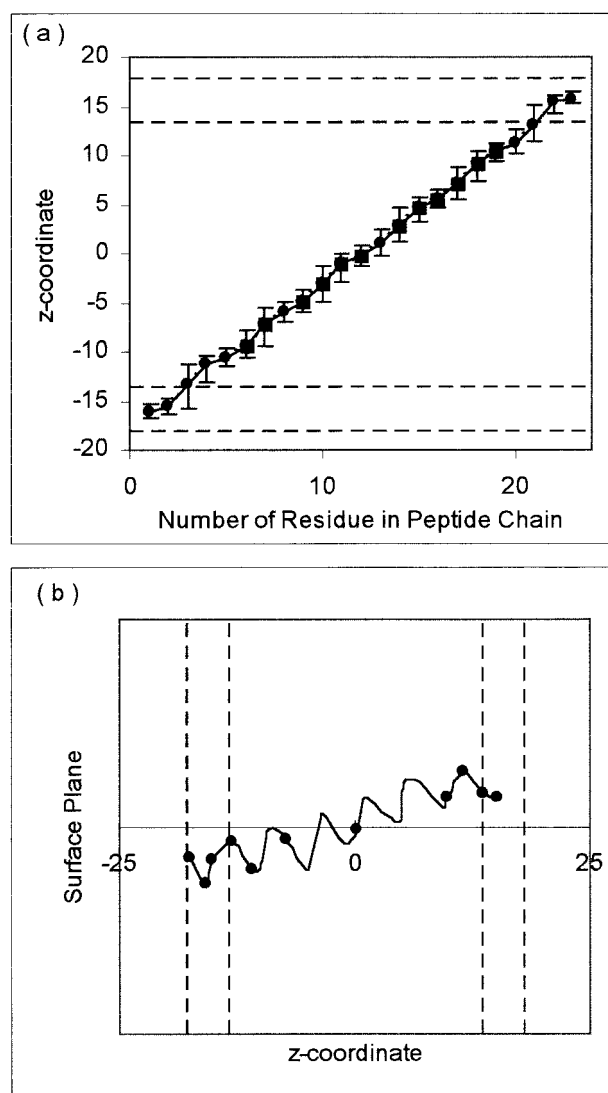


FIGURE 9 Inserted M2 $\delta$ . (a) residue *z*-coordinate ranges, and (b) a representative equilibrium configuration. Squares denote nonpolar residues, circles denote polar residues. Dashed lines indicate the head regions.

Continued insertion, followed by the realignment of the other end creates a fully extended helix (Fig. 11 *c*) that is free to rotate until it locates the head region and forms a trans-bilayer helix (Fig. 11 *d*).

For the 17 observed insertions, Table 3 shows the distribution of mechanism types for each tail polarity. Mechanisms in which the N-terminus inserts are listed separately from those in which the C-terminus inserts. The total numbers of each type of mechanism are also given. These results indicate that type I insertion is favored for bilayers with an octanol-like tail region ( $f_q = 0.65$ ), but type II insertion is more likely for all other tail polarities. For  $f_q \geq 0.80$ , only type II mechanisms are observed. Overall, N-terminus insertion is more common (70% of insertions), but C-terminus insertion also occurs, and the choice appears to be independent of bilayer tail polarity.

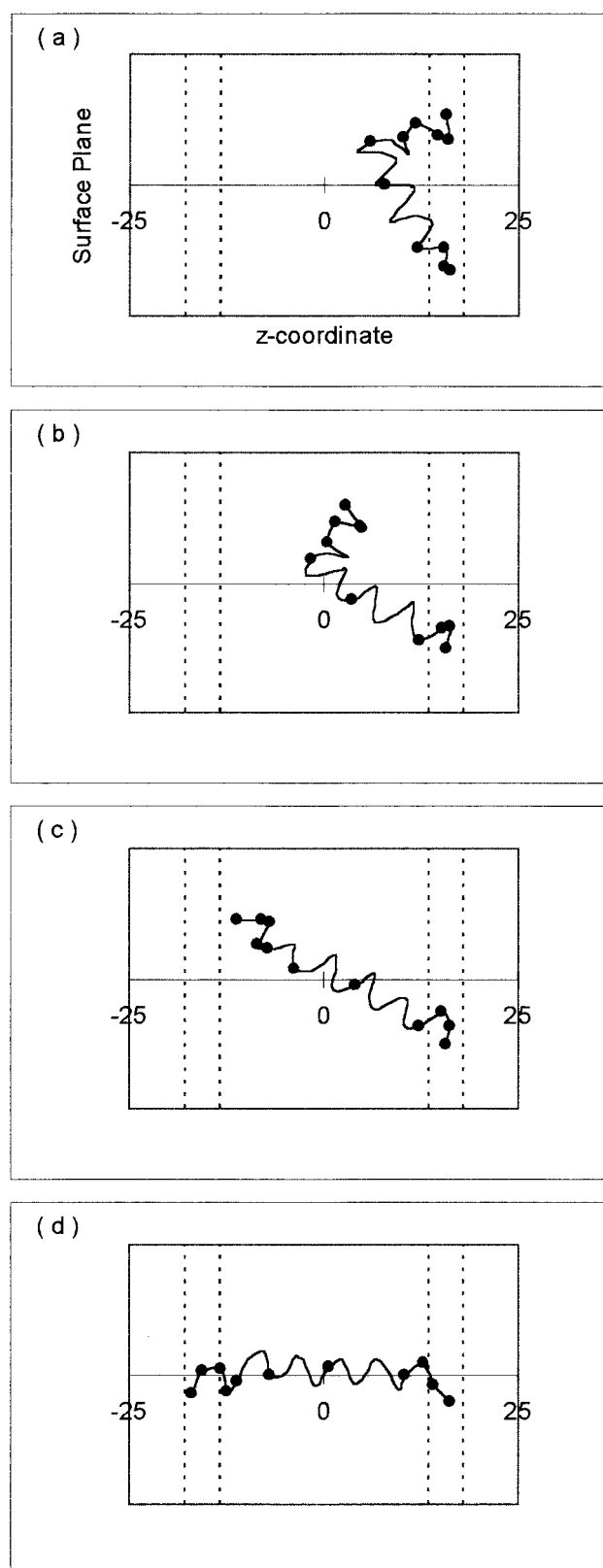


FIGURE 10 Snapshots from an M2 $\delta$  type I insertion mechanism (circles denote polar residues and vertical dotted lines show bilayer head regions). (a) MC step 1,260,000, (b) MC step 1,272,000, (c) MC step 1,350,000, (d) MC step 1,360,000.

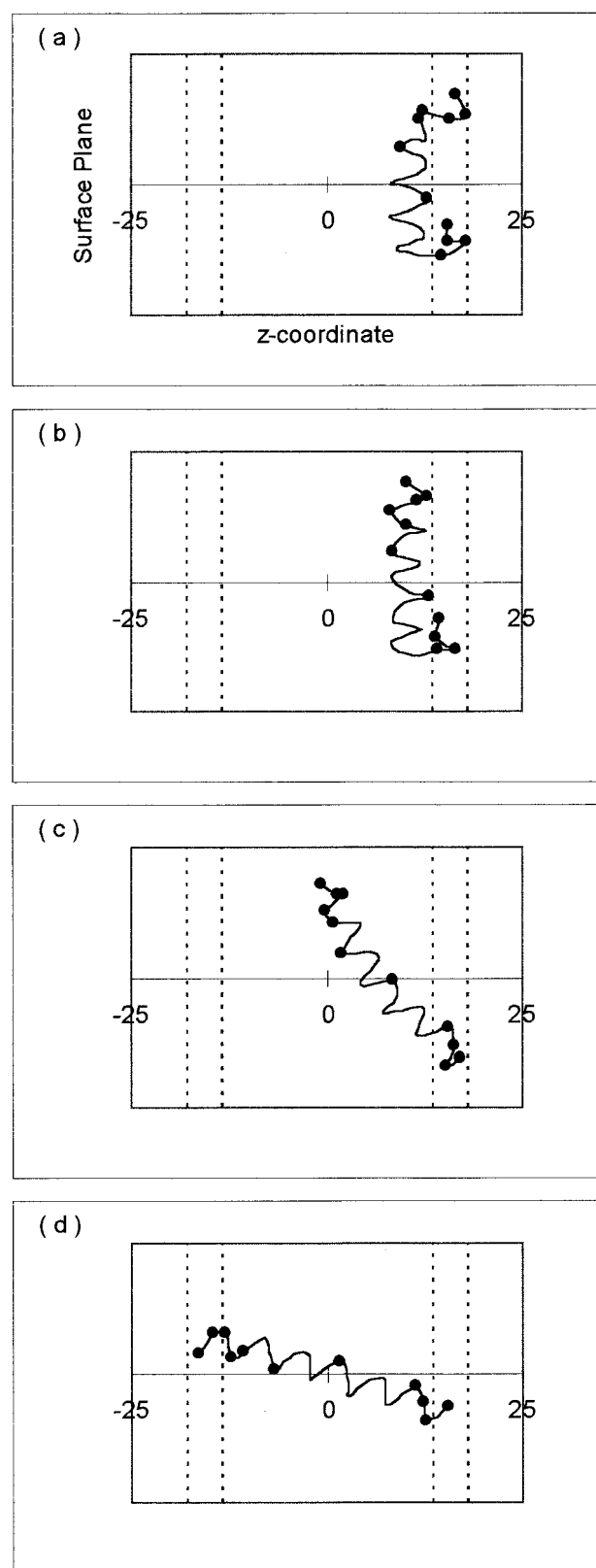


FIGURE 11 Snapshots from an M2 $\delta$  type II insertion mechanism (circles denote polar residues and vertical dotted lines show bilayer head regions). (a) MC step 27,160,000, (b) MC step 27,165,000, (c) MC step 27,212,000, (d) MC step 27,220,000.

**TABLE 3** The frequencies of type I and II insertion of M2 $\delta$ , for a range of bilayer tail polarities

$f_q$	N-terminus insertion		C-terminus insertion		Total	
	Type I	Type II	Type I	Type II	Type I	Type II
0.65	2	1	1	–	3	1
0.70	1	2	–	1	1	3
0.75	1	2	1	1	2	3
0.80	–	2	–	–	–	2
0.85	–	1	–	–	–	1
0.90	–	–	–	1	–	1

Although both mechanisms are multi-step processes, each step having its own energy barrier composed of thermodynamic and kinetic contributions, it is useful to approximate each mechanism to a single-step process, with one energy barrier to insertion. In this approximation, type I insertion has a larger thermodynamic contribution to its energy barrier than type II, but type II insertion has a larger kinetic contribution. As a result, the relative heights of the type I and II energy barriers are system dependent. For bilayers with octanol-like tail polarity ( $f_q = 0.65$ ), the kinetic contribution dominates, because the thermodynamic contribution is small, and M2 $\delta$  readily inserts via both mechanisms. The kinetic contribution to type I insertion is smaller than that of type II, so type I insertion is more likely for this bilayer. For bilayers with lower tail polarities, the kinetic contribution remains essentially unchanged whereas the thermodynamic contribution to the energy barriers increases. The thermodynamic contribution now dominates the insertion process. As a result, because type II insertion has a lower energy barrier than type I, type II insertion is favored for  $f_q = 0.70$  and  $0.75$  (although type I insertion still occurs). Beyond  $f_q = 0.75$ , the energy barrier to type I insertion is large enough to prevent insertion altogether (or at least make it very unlikely), whereas the type II energy barrier remains surmountable up to at least  $f_q = 0.90$ .

### N-terminus insertion

The preference for N-terminus insertion, regardless of mechanism type or bilayer tail polarity, can be explained by considering the residues at each end of M2 $\delta$ . In addition to the sum total polarity being slightly higher at the C-terminus, the last residue at that end is arganine. Arganine is extremely polar ( $q_o = -7.58$ ), and the energy barrier to its insertion will be higher than that of any residue at the N-terminus, under any conditions. Although not high enough to prevent C-terminus insertion altogether, this energy barrier difference is enough to make N-terminus insertion more likely.

### Magainin2 translocation

Figure 12 shows a series of simulation snapshots taken from a simulation of Magainin2 (at  $f_q = 0.65$ ) in which the peptide passes through the membrane. This behavior, called translocation, was only observed in simulations involving the most polar bilayer, with octanol-like tail polarity. Translocation occurred in four out of ten simulations at this tail polarity, the C-terminus leading in three out of four cases. Figure 12 *a* shows Magainin2 in its equilibrium conformation. For a sufficiently polar tail region, insertion of one end of the peptide is occasionally possible, producing a partially inserted, metastable structure (Fig. 12 *b*). Initial C-terminus insertion leads to a lower energy structure than N-terminus insertion, and is therefore favored for this first step, and, consequently, for the entire process. The noninserted end then aligns itself with the rest of the peptide (Fig. 12 *c*). A rotation of the extended helix follows, causing the peptide to fully insert (Fig. 12 *d*). A trans-bilayer helix is briefly formed when the inserted end enters the opposite head region, but the instability of Magainin2 in the trans-bilayer form leads to rapid insertion of the other end into the tail region (Fig. 12 *e*). It should be noted that the trans-bilayer form can also revert to the initial adsorbed conformation, rather than forming a translocated version. The extended helix then rotates until the original equilibrium structure is reproduced at the opposite side of the bilayer (Fig. 12 *f*). As noted above, translocation of Magainin2 is only observed when our model bilayers have an octanol-like tail region. For bilayers with less polar tail regions, the energy barriers to insertion of the polar residues, particularly lysine ( $q_o = -5.49$ ), are simply too large to overcome at 305 K.

Although we have only considered translocation of a small peptide, our observations may help to explain the insertion mechanisms of large membrane proteins. In their membrane conformation, these proteins consist of many trans-bilayer helices connected by polar segments, some of which have passed through the membrane, despite the energy barriers to insertion of polar residues. Although it would appear difficult for such segments to translocate without assistance, we have shown that, under the right circumstances, a peptide with limited stability in any inserted form can pass completely through a lipid bilayer.

### CONCLUSIONS

We have presented an essentially novel, semi-empirical lipid bilayer model, which interacts with a chain-of-spheres representation of two peptides in agreement with experimental observations (Bechinger et al., 1991). Without fitting parameters to these particular membrane/peptide systems, our model Magainin2 lies in, and approximately parallel to, the surface of the bilayer, whereas the model M2 $\delta$  inserts, forming a stable trans-bilayer helix that is approximately perpendicular to the surface. The same gen-

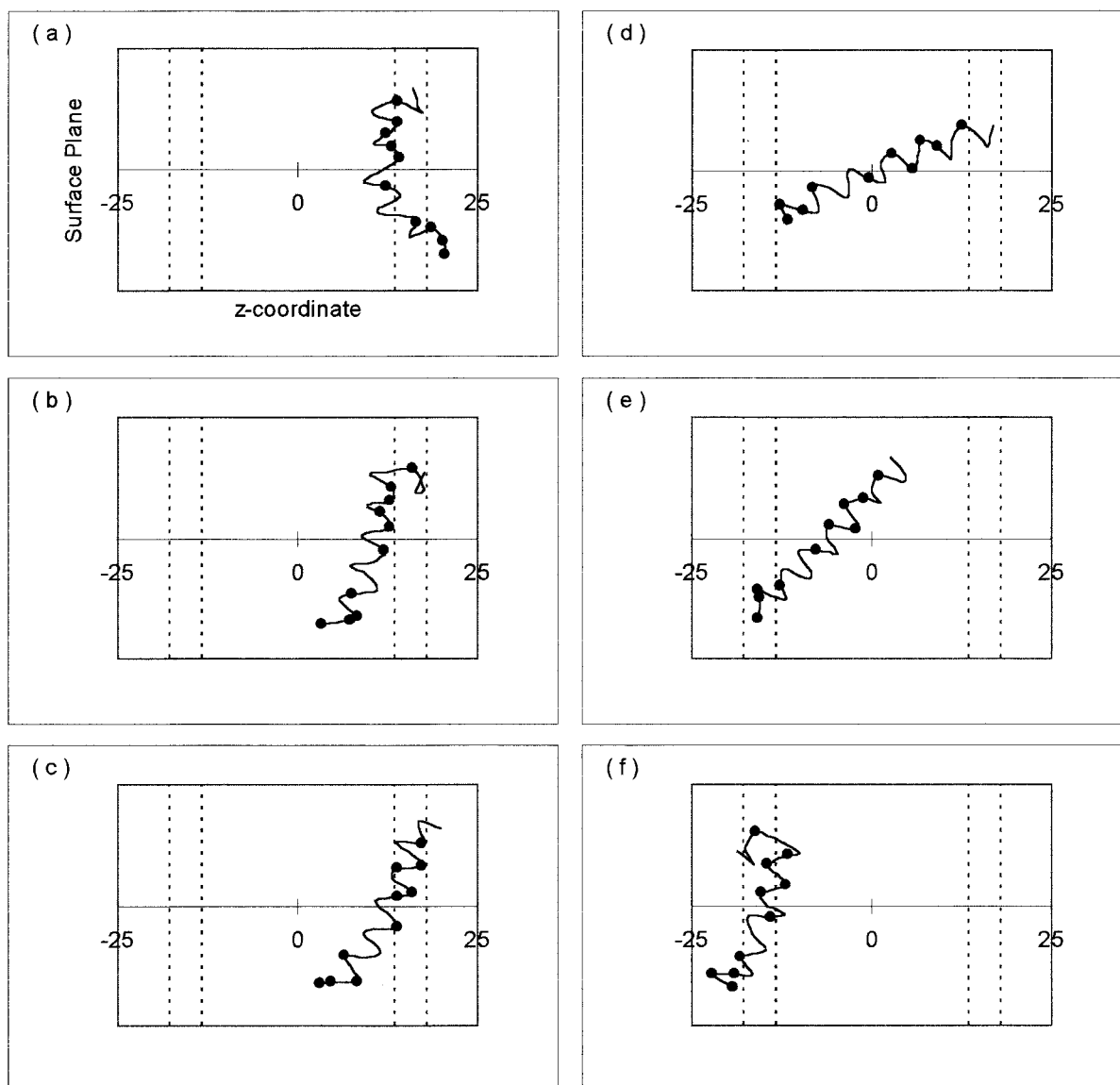


FIGURE 12 Snapshots from a Magainin2 translocation mechanism (circles denote polar residues and vertical dotted lines show bilayer head regions). (a) MC step 5,504,000, (b) MC step 5,550,000, (c) MC step 5,600,000, (d) MC step 5,651,000, (e) MC step 5,850,000, (f) MC step 5,900,000.

eral behavior of both Magainin2 and M2 $\delta$  has previously been modeled by Milik and Skolnick (1993) using a similar approach, but with some important differences. In particular, their parameter set was chosen pragmatically because it “work[s] in the present schematic model” (Milik and Skolnick, 1993), which could be expected to limit the utility of their model. Detailed studies of our model have enabled us to investigate equilibrium properties of the membrane/peptide systems, and characterize two different mechanistic pathways for the insertion of M2 $\delta$ , and one for the translocation of Magainin2.

Our model predicts that the M2 $\delta$  trans-bilayer helix will be at a slight angle to the  $z$  axis (which is perpendicular to the membrane surface), in agreement with the results of

Milik and Skolnick (1993). However, our model suggests that the center residues of Magainin2 will be more deeply adsorbed into the bilayer than its ends, the opposite of the conformation predicted by Milik and Skolnick (1993). Additionally, we have characterized a metastable equilibrium state for our model M2 $\delta$  that forms a helical hairpin at the membrane surface.

Insertion of our model M2 $\delta$  proceeds via two distinct mechanisms, each of which follows the general pathway predicted by Engelman et al. (1986), in which a randomly conformed peptide adsorbs to the bilayer surface, and at least partially self-assembles into a helical structure, before inserting into the bilayer interior. The type I insertion mechanism is kinetically favored, having fewer intermediate



states, whereas the type II mechanism is thermodynamically favored, having lower energy intermediate states. As a result, type I insertion is more likely in bilayers with octanol-like tail polarity, and type II insertion is more likely in bilayers with more hydrophobic tail regions. Type I insertion was never observed in bilayers with tail polarities of  $f_q > 0.75$ .

In addition to reproducing the noninserting equilibrium behavior of Magainin2, our simulations suggest that this peptide is able to translocate through one model bilayer ( $f_q = 0.65$ ) in the absence of an active membrane transport system. This behavior has not been predicted elsewhere, and there is currently no experimental verification available, although this may be due in part to the lower polarity of most membranes (relative to our model at  $f_q = 0.65$ ), which we would expect to hinder the translocation process.

Although one of our goals was to find an appropriate tail polarity for future theoretical models of a lipid bilayer, we were unable to do so unequivocally. The only model bilayer that did not reproduce the experimental observations for both Magainin2 and M2 $\delta$  was the one with alkane-like tail polarity. M2 $\delta$  was unable to insert into this bilayer, but even this result may be due to computational limitations rather than thermodynamic or kinetic factors. We therefore conclude that all tail polarities within our chosen range should be considered in future work, although  $f_q = 0.85$  corresponds most closely to experimental observations of the lipid bilayer tail region, which exhibits octanol-like and alkane-like behavior (Griffith et al., 1974; Stein 1986; Roseman, 1988a).

Strictly speaking, MC simulations do not take place in real time, but the strong correlation between consecutive configurations in the canonical ensemble allows us to draw reasonable conclusions about the simulation timescale. The approximate timescale for the M2 $\delta$  insertion seen in our simulations is extremely small. Even a complete 50-million-step simulation probably covers only a tiny fraction of a second in the life of the real system. Therefore, whenever a model peptide inserts, even if it does so in just one out of ten simulations, we would expect rapid insertion to be observed on an experimental timescale.

We have reproduced the experimentally observed insertion behavior of M2 $\delta$ , but have made no inference regarding its ability to lyse a membrane. This is because lysing requires an accumulation of peptides in the membrane, whereas our model currently considers only a single peptide. Possible mechanisms include the asymmetrical insertion of multiple peptides, leading to uneven stretching of the membrane (Longo et al., 1997, 1998), or the formation of peptide pore structures either before or after insertion (Kersch et al., 1989; White, 1992). We therefore leave open the question of lysing until we have completed investigations of a lipid bilayer model interacting with multiple peptides.

Previous simulations have used an orientational potential (Milik and Skolnick, 1993), or an array of hard cylinders (Baumgaertner, 1996) to persuade inserted peptides to orient themselves perpendicular to the bilayer surface, and thus span the membrane. In both cases, internal hydrogen bonding was assumed to be identical for all residues. In reality, and in our model, the end residues have incomplete internal hydrogen bonding in a perfect  $\alpha$ -helix. As a result, the end residues of our model peptide prefer to remain outside the tail region, where they can form external hydrogen bonds with water molecules. For peptides that are long enough to span the bilayer, the preference of each end for the head region determines the trans-bilayer orientation. Although the bilayer tails, which are physically absent from our model, probably influence the orientation of an inserted peptide to some degree, we believe this effect to be much smaller than the hydrogen-bonding effect. In addition, our model does not discourage a trans-bilayer peptide from assuming an orientation that is other than perpendicular to the bilayer surface. We have shown, in fact, that the peptide orientation in our model is a function of the peptide length and bilayer thickness, and that all observed trans-bilayer helices, on average, tilted slightly away from the perpendicular to the bilayer surface. Tilts of the same magnitude have also been reported in experimental studies of HIV-1 and influenza peptides (Bechinger, 2000), and in an MD study of the amphiphilic helical peptide, ace-K2GL16K2A-amide (Belohorcova et al., 1997).

A further prediction from our simulations is that a critical bilayer thickness exists (39 Å), above which M2 $\delta$  will not insert at all. As previously noted, this value should not be directly compared to the equilibrium thickness of real bilayers, which, unlike our model, deform as a result of peptide insertion. This deformation can include bending, stretching, thickening, or thinning of the bilayer, with an associated increase or decrease in energy (the membrane-deformation energy). The balance between the Gibbs energy of deformation and the Gibbs energy of peptide insertion dictates whether the membrane will deform to support a trans-bilayer conformation (the Gibbs energy includes enthalpy and entropy terms). In a real system, the critical thickness therefore corresponds to a bilayer in which the sum of the membrane-deformation energy and the trans-bilayer peptide-insertion energy is zero. The energy required for sufficient membrane deformation (largely acyl chain contraction) in a thicker bilayer would be greater than the energy gained by the formation of a trans-bilayer helix. For a thickness mismatch of this type, the trans-bilayer insertion of our model peptide is energetically unfavorable, in general agreement with the results of Dan and Safran (1995).

Of course, the model has certain limitations. Being an effective medium approximation, the bilayer has no physical structure and therefore takes no account of lipid properties such as bending stiffness, spontaneous curvature, lipid

density, and other steric effects that might hinder, or even help insertion. Without physical lipid tails, the model cannot account for entropy changes associated with tail disordering upon insertion of a peptide chain, and the peptide model itself is a coarse approximation of a real residue chain. However, by using empirical partitioning and transfer data, and fitting the bilayer functions to experimental results of model tripeptides, many of the limitations are accounted for within the parameters of the model. The use of empirical data does limit the pH and temperature of our simulations to those at which the data were taken (pH 7.0 and 305 K), but, provided the empirical data are available, the model may be used with a different parameter set to simulate any pH and temperature. In fact, pH variation may be particularly interesting for systems in which a pH change acts as a mechanistic trigger, such as the invasion of cells by the influenza virus. In this example, the acidic environment of the cellular endosome triggers a conformational change in the hemagglutinin protein, switching it to a fusogenic from a nonfusogenic structure (Carr et al., 1997).

In conclusion, our simulations suggest that the current model is a good qualitative representation of a membrane/peptide system. It can be used to investigate the microscopic details of systems with known macroscopic behavior, including nonequilibrium insertion and translocation mechanisms, to test and formulate hypotheses that would assist and direct future experimental research. The model might also be useful as a predictive tool for screening large numbers of peptides and protein fragments, or to study particular membrane/peptide combinations that present experimental difficulties.

## APPENDIX A

Three types of micromodifications (system perturbations) are used to generate new peptide conformations, and hence new system configurations:

1. Peptide translation: The whole peptide is moved a small, random distance (between 0 and 0.2 Å) along each Cartesian axis.
- 2a. Spike move (end residue): The virtual bond connected to the end residue is rotated slightly in the  $xy$  plane and then in the  $yz$  plane (a random angle between 0 and 20° is used for each rotation).
- 2b. Spike move (central residue): While all other residues remain fixed in space, and all virtual bond lengths remain fixed, one randomly chosen residue is rotated a small, random amount (between 0 and 20°) around an axis joining the centers of its two nearest neighbors.
3. Slide move: A virtual bond is randomly chosen, and all residues on one side of it (the side is chosen randomly) are translated a small, randomly chosen distance through space (between 0 and 0.2 Å), while remaining fixed relative to each other. At the end of the move, the chosen virtual bond is unchanged in length, but has rotated relative to the residues it connects.

A single MC step consists of one modification of each type, 1, 2 (a or b depending on which residue is chosen), and 3. After each modification, the new energy of the system is calculated, and hence the energy change due to the modification. A modification is "accepted" (i.e., the new configuration becomes the current configuration), if the Boltzmann factor

of the energy change is greater than a random number,  $\eta$ , taken from a uniform distribution between 0 and 1,

$$\exp\left(\frac{-\Delta U}{RT}\right) > \eta. \quad (\text{A1})$$

Any configurational change with a negative  $\Delta U$  has a Boltzmann factor greater than 1 and is always accepted. Configurational changes with a positive  $\Delta U$  and a Boltzmann factor between 0 and 1 have varying probabilities of acceptance, depending on the size of  $\Delta U$ —a Boltzmann factor of 0.9 is accepted 9 out of 10 times, whereas a Boltzmann factor of 0.01 is only accepted 1 out of 100 times. Therefore, the system will usually change to minimize its energy, but the possibility of a positive energy change allows the system to escape local minima, and implicitly include the entropy in the minimization. This last point is particularly important, because including the entropy causes the Gibbs energy, rather than just the enthalpy to be minimized. Using only these three types of micromodification, the peptide is able to rapidly change conformation and location to minimize the Gibbs free energy of the system.

## APPENDIX B

The locations of the functions,  $w(z)$  (fractional water content) and  $y(z)$  (hydrophobicity), along the  $z$  coordinate are given by  $w_{\text{shift}}$ ,  $y_{\text{shift1}}$ , and  $y_{\text{shift2}}$ . These parameters were fitted to the experimentally observed adsorption behavior of a series of tripeptides interacting with a lipid bilayer at 303 K (Jacobs and White, 1989). In their study, each tripeptide was of the form Ala-X-Ala-*O-tert*-butyl, where X was Gly (G), Ala (A), Leu (L), Phe (F), or Trp (W). Equilibrium dialysis was used to measure partition functions, and density profiles were generated using neutron diffraction.

The experimental results showed that all the tripeptides adsorbed into the bilayer, spending over 80% of their time near the midplane of the head region. However, only 56% of the expected water-to-alkane transfer energy was released upon adsorption, and none of the tripeptides inserted into the bilayer tail region. It was concluded that adsorption into the head region (interfacial binding), is determined principally by the hydrophobic effect, and that polar interactions remain largely satisfied within the head region (the latter conclusion was our basis for choosing  $p_{\text{shift}} = -1.5$  Å). Because the behavior of the tripeptides is unaffected by the polarity function,  $p(z)$ , only the other two bilayer functions,  $w(z)$  and  $y(z)$ , could be fitted to the experimental tripeptide data.

After running many test simulations using different combinations of  $w_{\text{shift}}$ ,  $y_{\text{shift1}}$ , and  $y_{\text{shift2}}$ , a good fit to the experimental tripeptide data was achieved using  $w_{\text{shift}} = 1.65$  Å,  $y_{\text{shift1}} = -1.5$  Å, and  $y_{\text{shift2}} = 3.0$  Å. A set of longer runs was then completed to provide more accurate data in support of these parameters. Five simulations of 50 million MC steps were run for tripeptides with X = G and F, and four simulations of 50 million MC steps were run for tripeptides with X = A, L, and W. The temperature was set at 305 K, and the initial configuration was a random coil in the aqueous phase. In each case, the *-O-tert*-butyl group was treated as a fourth hard sphere attached to the tripeptide chain, with an accessible surface area twice that of CH<sub>3</sub> (Reynolds et al., 1974; Harris et al., 1973), so that  $b_0(-O\text{-tert-butyl}) = -3.21$  kcal/mol, and  $b_1(-O\text{-tert-butyl}) = q_0(-O\text{-tert-butyl}) = 0$ .

Our simulations showed that, for all values of  $-X-$ , the tripeptide spent most of its time in the center of the head region, with the  $z$ -coordinate probability distribution peak lying between 16.2 and 16.6 Å from the center of the bilayer (the head region is between 13.5 and 18 Å from the center). As expected, the tripeptide does not insert into the tail region, either experimentally, or in our simulation. This is because internal hydrogen bonds may only form between fourth-nearest neighbors along the peptide chain (third- and fourth-nearest neighbors are included in our helicity factor,  $V_H(r_n)$ ), and a tripeptide has no more than second-nearest neighbors. In the absence of internal hydrogen bonding, the water content function,  $w(z)$ , acts as a barrier to tripeptide insertion into the tail region. It should

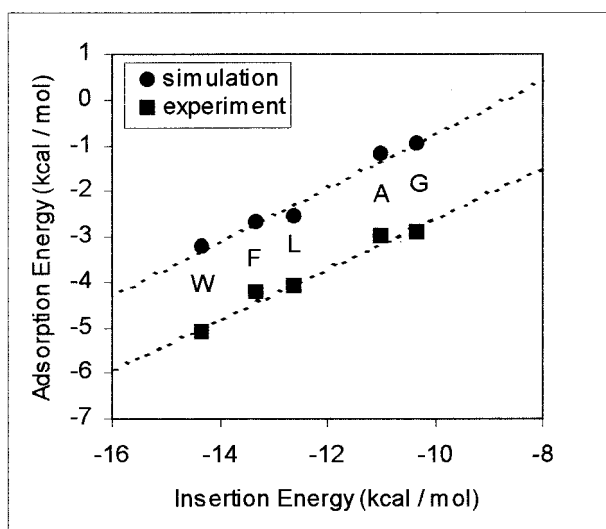


Figure B1 Theoretical insertion energy plotted against experimental and simulated adsorption energy for five tripeptides.

be noted, however, that the tripeptide was quite mobile during the simulation, spending time in the aqueous phase and in the head region, i.e., the adsorption is reversible. For an experimental system in which a large number of tripeptide molecules are present, equilibrium partitioning would be observed between the aqueous phase and the bilayer. Therefore, to compare experiment and simulation, our equilibrium energy change is an average over adsorbed and desorbed states.

Figure B1 shows the equilibrium energy change of each tripeptide upon adsorption into the head region (adsorption energy) along the  $y$  axis, and the expected water-to-alkane transfer energy (insertion energy) along the  $x$  axis (Jacobs and White, 1989). Circles indicate simulation results, squares indicate experimental results, and the five  $-X-$  residue types are indicated by their single-letter abbreviations. The simulation points have standard deviations between 3 and 6% of their values, which is less than the size of the circles. For both sets of data, the points lie approximately along a straight line. The slope of this line indicates the percentage of the expected transfer energy that is realized upon adsorption into the head region, and our fitted model must therefore reproduce the slope of the experimental data. A least-squares linear regression of the experimental data yields a slope of  $0.56 \pm 0.05$ , whereas a similar linear regression for the simulation data yields a slope of  $0.59 \pm 0.04$  (linear regressions shown as dotted lines). These values are the same within estimated errors, and so the chosen  $w_{\text{shift}}$ ,  $y_{\text{shift}1}$ , and  $y_{\text{shift}2}$  parameters successfully reproduce the experimental adsorption energy percentage and the location of the adsorbed tripeptides.

It should be noted that the  $y$  intercept should not be used to compare experimental and simulation results. This value gives an estimate of non-hydrophobic terms, including peptide immobilization effects, peptide conformational changes, and lipid perturbation effects (Jacobs and White, 1989). The last of these terms will clearly be absent from our results, because there are no lipid molecules present in our model. The other terms, which are largely entropic, are accounted for implicitly by the MC simulation technique, and therefore do not contribute to the measured energy of the system. As expected, these differences in the way the adsorption energy is calculated result in different  $y$ -axis intercepts for the experimental and simulation data, which do not affect the parameter fitting.

It should also be noted that the measured surface adsorption energy (approximately 56% of the expected water-to-alkane transfer energy), is not simply the water-to-surface transfer energy for residues, but rather a combination of this partial-transfer energy, and a surface-deformation energy due to bending, stretching, or rearrangement of the bilayer mole-

cules as a result of peptide adsorption. Although it is not possible to isolate the bilayer deformation energy, it is nevertheless included implicitly within our model.

This work was supported by the National Science Foundation through the CAREER Program (BES-9733764). This work was supported by the Materials Research Science and Engineering Center program of the National Science Foundation under Award DMR-9808677.

We would also like to thank Tim Ratto and Belinda Bashore for their computational help.

## REFERENCES

- Allen, M. P., and D. J. Tildesley. 1989. *Computer Simulation of Liquids*. Clarendon Press, Oxford, UK. 110–123.
- Barlow, D. J., and J. M. Thornton. 1988. Helix geometry in proteins. *J. Mol. Biol.* 201:1248–1255.
- Baumgaertner, A. 1996. Insertion and hairpin formation of membrane proteins: a Monte Carlo study. *Biophys. J.* 71:1248–1255.
- Bechinger, B., Y. Kim, L. E. Chirlian, J. Gessel, J.-M. Neumann, M. Montal, J. Tomich, M. Zasloff, and S. J. Opella. 1991. Orientations of amphiphilic helical peptides in membrane bilayers determined by solid state NMR spectroscopy. *J. Biomol. NMR.* 1:167–173.
- Bechinger, B. 2000. Biophysical investigations of membrane perturbations by polypeptides using solid-state NMR spectroscopy (review). *Mol. Membrane Biol.* 17:135–142.
- Belohorcova, K., J. H. Davis, T. B. Woolf, and B. Roux. 1997. Structure and dynamics of an amphiphilic peptide in a lipid bilayer: a molecular dynamics study. *Biophys. J.* 73:3039–3055.
- Ben-Shaul, A., N. Ben-Tal, and B. Honig. 1996. Statistical thermodynamic analysis of peptide and protein insertion into lipid membranes. *Bio-phys. J.* 71:130–137.
- Berneche, S., N. Mafalda, and B. Roux. 1998. Molecular dynamics simulation of melittin in a dimyristoylphosphatidylcholine bilayer membrane. *Biophys. J.* 75:1603–1618.
- Biggin, P. C., and M. S. P. Sansom. 1999. Interactions of  $\alpha$ -helices with lipid bilayers: a review of simulation studies. *Biophys. Chem.* 76: 161–183.
- Cantor, R. S. 1999. Solute modulation of conformational equilibria in intrinsic membrane proteins: apparent “cooperativity” without binding. *Biophys. J.* 77:2643–2647.
- Carr, C. M., C. Choudry, and P. S. Kim. 1997. Influenza hemagglutinin is spring-loaded by a metastable native conformation. *Proc. Natl. Acad. Sci. U.S.A.* 94:14306–14313.
- Channareddy, S., and N. Janes. 1999. Direct determination of hydration in the interdigitated and ripple phases of dihexadecylphosphatidylcholine: hydration of a hydrophobic cavity at the membrane/water interface. *Biophys. J.* 77:2046–2050.
- Chou, T., K. S. Kim, and G. Oster. 2001. Statistical thermodynamics of membrane bending-mediated protein–protein attractions. *Biophys. J.* 80: 1075–1087.
- Dan, N., and S. A. Safran. 1995. Solubilization of proteins in membranes. *Israel J. Chem.* 35:37–40.
- Dan, N. 1996. Formation of ordered domains in membrane-bound DNA. *Biophys. J.* 71:1267–1272.
- Dan, N., and S. A. Safran. 1998. Effect of lipid characteristics on the structure of transmembrane proteins. *Biophys. J.* 75:1410–1414.
- Efremov, R. G., D. E. Nolde, G. Vergoten, and A. S. Arseniev. 1999a. A solvent model for simulations of peptides in bilayers. I. Membrane-promoting  $\alpha$ -helix formation. *Biophys. J.* 76:2448–2459.
- Efremov, R. G., D. E. Nolde, G. Vergoten, and A. S. Arseniev. 1999b. A solvent model for simulations of peptides in bilayers. II. Membrane-spanning  $\alpha$ -helices. *Biophys. J.* 76:2460–2471.

- Engelman, D. M., and T. A. Steitz. 1981. The spontaneous insertion of proteins into and across membranes: the helical hairpin hypothesis. *Cell*. 23:411–422.
- Engelman, D. M., T. A. Steitz, and A. Goldman. 1986. Identifying non-polar transbilayer helices in amino acid sequences of membrane proteins. *Annu. Rev. Biophys. Biophys. Chem.* 15:321–353.
- Gregoret, L. M., and F. E. Cohen. 1990. Novel method for the rapid evaluation of packing in protein structure. *J. Mol. Biol.* 211:959–974.
- Griffith, O. H., P. H. Dehlinger, and S. P. Van. 1974. Shape of the hydrophobic barrier of phospholipid bilayers (evidence for water penetration). *J. Membr. Biol.* 15:159–192.
- Harris, M. J., T. Higuchi, and J. H. Ritting. 1973. Thermodynamic group contributions from ion pair extraction equilibria for use in the prediction of partition coefficients. Correlation of surface area with group contributions. *J. Phys. Chem.* 77:2694–2703.
- Ho, C., S. J. Slater, and C. D. Stubbs. 1995. Hydration and order in lipid bilayers. *Biochemistry*. 34:6188–6195.
- Jacobs, R. E., and S. H. White. 1989. The nature of hydrophobic binding of small peptides at the bilayer interface: implications for the insertion of transbilayer helices. *Biochemistry*. 28:3421–3437.
- Jain, M. K., J. Rogers, L. Simpson, and L. M. Gierasch. 1985. Effect of tryptophan derivatives on the phase properties of bilayers. *Biochim. Biophys. Acta*. 816:153–162.
- Kersch, G. J., J. M. Tomich, and M. Montal. 1989. The M28 transmembrane domain of the nicotinic cholinergic receptor forms ion channels in human erythrocyte membranes. *Biochem. Biophys. Res. Commun.* 162:352–356.
- Klotz, I. M., and S. B. Farnham. 1968. Stability of an amide–hydrogen bond in an apolar environment. *Biochemistry*. 7:3879–3882.
- Kresheck, G. C., and I. M. Klotz. 1969. The thermodynamics of transfer of amides from an apolar to an aqueous solution. *Biochemistry*. 8:8–12.
- Lin, J.-H., and A. Baumgaertner. 2000. Adsorption of melittin to a lipid bilayer: a molecular dynamics study. *J. Mol. Liquids*. 84:89–98.
- Longo, M. L., A. J. Waring, and D. A. Hammer. 1997. Interaction of the influenza hemagglutinin fusion peptide with lipid bilayers: area expansion and permeation. *Biophys. J.* 73:1430–1439.
- Longo, M. L., A. J. Waring, L. M. Gordon, and D. A. Hammer. 1998. Area expansion and permeation of phospholipid membrane bilayers by influenza fusion peptides and melittin. *Langmuir*. 14:2385–2395.
- McIntosh, T. J., and S. A. Simon. 1993. Contributions of hydration and steric (entropic) pressures to the interactions between phosphatidylcholine bilayers: experiments with the subgel phase. *Biochemistry*. 32:8374–8384.
- Milik, M., and J. Skolnick. 1992. Spontaneous insertion of polypeptide chains into membranes: a Monte Carlo model. *Proc. Natl. Acad. Sci. U.S.A.* 89:9391–9395.
- Milik, M., and J. Skolnick. 1993. Insertion of peptide chains into lipid membranes: an off-lattice Monte Carlo dynamics model. *Proteins Struct. Funct. Genet.* 15:10–25.
- Milik, M., and J. Skolnick. 1995. A Monte Carlo model of fd and Pf1 coat proteins in lipid membranes. *Biophys. J.* 69:1382–1386.
- Nicol, F., S. Nir, and F. C. Szoka. 2000. Effect of phospholipid composition on an amphipathic peptide-mediated pore formation in bilayer vesicles. *Biophys. J.* 78:818–829.
- Reynolds, J. A., D. B. Gilbert, and C. Tanford. 1974. Empirical correlation between hydrophobic free energy and aqueous cavity surface area. *Proc. Natl. Acad. Sci. U.S.A.* 71:2925–2927.
- Richards, F. M. 1977. Areas, volumes, packing, and protein structure. *Annu. Rev. Biophys. Bioeng.* 6:151–176.
- Rose, G. D., A. R. Geselowitz, G. J. Lesser, R. H. Lee, and M. H. Zehfus. 1985. Hydrophobicity of amino-acid residues in globular proteins. *Science*. 229:834–838.
- Roseman, M. A. 1988a. Hydrophilicity of polar amino acid side-chains is markedly reduced by flanking peptide bonds. *J. Mol. Biol.* 200:513–522.
- Roseman, M. A. 1988b. Hydrophobicity of the peptide C=O··H–N hydrogen-bonded group. *J. Mol. Biol.* 201:621–623.
- Sintes, T., and A. Baumgaertner. 1998. Membrane-mediated protein attraction. a Monte Carlo study. *Physica A*. 249:571–575.
- Stein, W. D. 1986. Transport and Diffusion Across Cell Membranes. Academic Press, New York.
- van Gunsteren, W. F., and M. Karplus. 1982. Effect of constraints on the dynamics of macromolecules. *Macromolecules*. 15:1528–1544.
- White, J. 1992. Membrane fusion. *Science*. 258:917–924.
- Zaslloff, M. 1987. Magainins, a class of antimicrobial peptides from *Xenopus* skin: isolation, characterization of two active forms, and partial cDNA sequence of a precursor. *Proc. Natl. Acad. Sci. U.S.A.* 84:5449–5453.
- Zhou, Z., J. C. Macosko, D. W. Hughes, B. G. Sayer, J. Hawes, and R. M. Epand. 2000. <sup>15</sup>N NMR study of the ionization properties of the influenza virus fusion peptide in zwitterionic phospholipid dispersions. *Biophys. J.* 78:2418–2425.